Susceptibility of 12% CR steels to sensitisation during welding of thick gauge plate

Martin Nicholas Van Warmelo
University of Wollongong

SUSCEPTIBILITY OF 12% CR STEELS TO SENSITISATION DURING WELDING OF THICK GAUGE PLATE

A thesis submitted in fulfilment of the requirements for the award of the degree of

MASTER OF ENGINEERING

(Materials Engineering)

from

THE UNIVERSITY OF WOLLONGONG

by

MARTIN NICHOLAS VAN WARMELO, BE

FACULTY OF ENGINEERING

2006

Declaration

I, Martin Nicholas van Warmelo, declare that this thesis, submitted in fulfilment of the requirements for the award of Master of Engineering, in the Faculty of Engineering, University of Wollongong, is wholly my own work unless otherwise referenced or acknowledged. The document has not been submitted for qualifications at any other academic institution.

Martin Nicholas van Warmelo, BE

Wednesday, 01 August 2007

Acknowledgements

This work could not have been completed without the support and assistance of numerous people and special thanks are due to the following people.

My project supervisors, Dr David Nolan and Prof John Norrish for their encouragement and assistance throughout the project.

Mr Jim Williams and Dr Frank Barbaro of Bluescope Steel who provided invaluable background information concerning problems encountered with sensitisation in coal wagons manufactured from 12 Cr steels.

Mr Peter Moore of Atlas Speciality Steels for financial support and materials.

Dr Peter Innis of the Intelligent Polymer Research Institute at the University of Wollongong for assistance with the electrochemical investigations

Numerous members of the technical staff at the University of Wollongong for assistance with sample preparation and machining but specifically Mr Greg Tillman for assistance with the metallography and Mr Bob de Jong for assistance on the Gleeble.

Lastly, but most significantly, my wife Sanet for her support, love and encouragement during a difficult transition period in our lives.

Abstract

In recent years, the subject of sensitisation in unstabilised ferritic/martensitic dual phase 11-14%Cr steels has been investigated in some detail after a number of failures in service due to accelerated corrosion. It was found that sensitisation could occur due to a number of different mechanisms which were dependant on the heat treatment, the number of thermal cycles and the phases present in the material. All the detected modes of sensitisation could be prevented by stabilisation with titanium or niobium and suitable design of the material composition to produce a suitably high ferrite factor. However, these options could not readily be applied to thick gauge plate and therefore 12%Cr material available in the market above 10mm thickness still tends to be unstabilised.

This project was initiated with the intention of determining how sensitisation would manifest itself during welding of thicker plates and whether the degree of sensitisation could be controlled to acceptable levels by appropriate control of the welding parameters. This was done in two phases, namely evaluation of actual welds produced using varying heat input parameters and by simulation of the thermal treatment using a Gleeble 3500 thermomechanical simulator. The samples were evaluated using standard immersion tests (Strauss test) and electrochemical techniques.

Mode 2 sensitisation was found to occur on all samples and on all materials, irrespective of the welding parameters. This occurred at all points where the heat affected zone (HAZ) from one weld bead intersected with the HAZ from a previous bead. However, the sensitised regions were generally well below the surface of the material and would

therefore not be exposed to the atmosphere and any corrosive environment. The exception to this rule occurred when very high heat input resulted in an excessively large HAZ or when poor weld bead positioning and inappropriate bead overlap resulted in sensitisation of the HAZ on the surface.

Mode 3 sensitisation did not occur within the range of welding parameters investigated.

Mode 4 sensitisation was found to occur on all materials but could not reliably be detected by the Strauss test. Electrochemical evaluation clearly showed that sensitisation was present in the subcritical HAZ on all materials, irrespective of welding conditions. However, the degree of sensitisation was very low.

From a practical perspective, problems in service due to sensitisation are most likely to arise from very high heat input levels and welding defects such as excessive overlap of weld beads and incomplete fusion.

Table of Contents

Table of Figures

List of Tables

Sensitisation of Thick Gauge 3CR12 Plate

1 Introduction

In recent years, sensitisation in 12%Cr steels was the subject of intensive investigation after several failures were reported in coal wagons in Australia. Work conducted at the BlueScope laboratories in Port Kembla determined that sensitisation could occur as a result of a number of different mechanisms, which will be discussed in detail at a later stage. The different mechanisms resulted in sensitisation manifesting itself after different heat treatments and at different positions relative to the weld bead.

The conclusions from the abovementioned studies were that sensitisation could only be totally eliminated by effective stabilisation using titanium or niobium additions and suitable control of the ferrite factor. However, these options did not offer a fully practical solution in the case of thick gauge plate and the majority of 12%Cr material on the Australian market is still unstabilised.

This investigation was initiated in an attempt to determine how severely thick gauge material was susceptible to sensitisation, how it would manifest itself in multiple pass welds and to what extent it could be minimised by appropriate control of the welding parameters.

2 Literature Survey

2.1 Sensitisation

2.1.1 Definition

Sensitisation in stainless steel (SS) can be defined as susceptibility to intergranular corrosion (IGC) which occurs due to the presence of chromium depleted zones at the grain boundaries. This depletion is generally associated with the precipitation of chromium carbides on the grain boundaries, which remove chromium from the matrix and reduce the corrosion resistance along the grain boundaries. In their simplest form, the carbides would be $Cr_{23}C_6$ or Cr_7C_3 which consume a large quantity of chromium on formation due to the high stoichiometric ratio.

2.1.2 Background

The mechanism of chromium depletion and the impact on reduced resistance to IGC was identified in austenitic stainless steels as far back as the 1930s by Bain et el [1] but it was only from the 1960s that the identical mechanism was identified by several researchers [2-6] as being the cause of sensitisation in ferritic stainless steels. As recently as the early 1970s, theories for sensitisation included preferential dissolution of iron-carbides, accelerated corrosion due to stresses induced by precipitates, the presence of austenite at grain boundaries or galvanic action between precipitates and the surrounding matrix [7]. It was not immediately obvious that the mechanism present in austenitic and ferritic steels was the same because the procedures used to remove sensitisation in austenitic stainless steels created a problem in ferritic stainless steels. Austenitic stainless steels sensitise during prolonged exposure to temperatures in the range between 400° and 800°C and the standard resistance to IGC can readily be

restored by heating the steel above 950°C and cooling rapidly. In contrast, ferritic stainless steels are highly susceptible to sensitisation after exposure to temperatures above 950°C and the corrosion resistance can be restored by heating in the temperature range 700° to 900°C [7, 8]. The extended time before the mechanism of sensitisation in ferritic stainless steels was identified was partly due to the fact that there was very little commercial interest in ferritic stainless steels until the 1960s. Until then, the commercially available ferritic stainless steels were plagued by problems of poor ductility and corrosion resistance, especially in a welded condition. Several researchers [6, 7, 9, 10] showed that these problems could be significantly improved by reducing the carbon and nitrogen levels in the steel, but at the time this could only be done with expensive vacuum induction melting processes. The development of the Argon/Vacuum Oxygen Decarburisation (AOD/VOD) processes led to renewed interest in ferritic stainless steels since these could now be produced competitively with combined [C+N] content below 0.03%.

2.1.3 Mechanism

As mentioned previously, sensitisation occurs when chromium carbides precipitate on grain boundaries, leaving a continuous chromium depleted zone which is more susceptible to corrosive attack. In order for a chromium depleted zone to form, there are two overriding requirements. These are that the carbon diffusion rate has to be sufficiently high for significant diffusion of carbon to the grain boundaries to occur and the chromium diffusion rate must be correspondingly low to prevent diffusion into the depleted zones. The large difference in the diffusion rate of carbon in austenite and ferrite is predominantly responsible for the disparity between the conditions which lead to sensitisation in ferritic and austenitic stainless steels

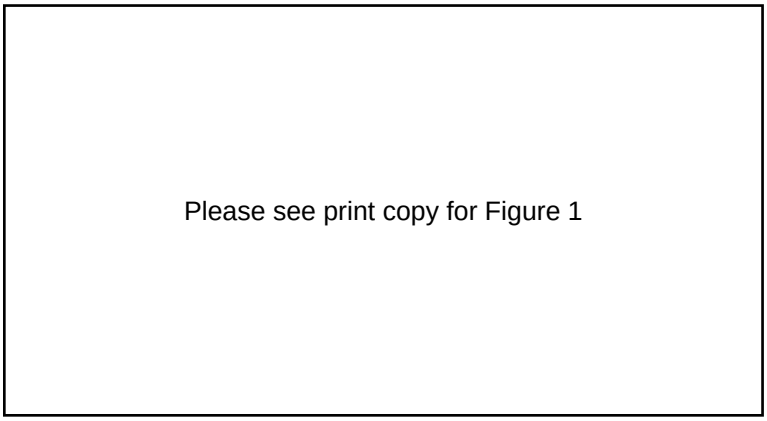

Figure 1 : Effect Of Steel Composition On Sensitising Behaviour (Sensitised Within Bounding Lines) [12]

A detailed theoretical analysis from a thermodynamic perspective was performed by Arai et al [14, 15] which showed that the precipitation rate in ferritic stainless steels is of the order of 10^6 times more rapid than in austenitic stainless steels [6, 11-13]. This is illustrated in Figure 1 [12] which shows the comparative times for ferritic and austenitic steels to become sensitised. While this may appear to contradict earlier statements that sensitisation in ferritic steels occurs on exposure to temperatures above 900°C, exposure to the elevated temperature is required to release carbon into solution, which would previously have been in the form of carbides. During subsequent exposure to temperatures illustrated in Figure 1, carbon diffusion to the grain boundaries with subsequent sensitisation will occur. The significantly higher solubility of carbon in austenite is also a determining factor, since the tendency to reject carbon from solid solution isn't as strong. However, carbides are not the only precipitates which can contribute to sensitisation. In ferritic stainless steels, nitrogen will also form chromium rich precipitates in the absence of thermodynamically more favourable alternatives but due to the high solubility of nitrogen in γ, nitrogen does not contribute significantly to sensitisation in austenitic stainless steels.

It has been shown [16] that the precipitates frequently contain complex carbo-nitrides and localised chromium concentrations can also be reduced by the formation of borides [17] and therefore any elements which can form chromium precipitates with subsequent chromium depletion on the grain boundaries can contribute to sensitisation. In a series of studies evaluating IGC in austenitic stainless steels using atomic force microscopy (AFM), Barkleit et al stated that IGC in low carbon austenitic stainless steels could be initiated by phosphorus segregation [18] or by high sulphur levels [19]. While it could be argued that the observed corrosion was attributable to dissolution of the precipitates or the precipitate/material interface, the authors maintain that AFM analysis could clearly distinguish between dissolution around precipitates and IGC. However, no detail concerning the actual mechanism of how the presence of sulphur or phosphorus causes chromium depletion and IGC is given. No equivalent study on ferritic stainless steels has been found.

Due to the slow carbon diffusion rate and the greater solubility, the tendency for carbide precipitation in austenitic steels is low and is only likely to occur at high carbon concentrations, very slow cooling rates or extended exposure to the sensitising temperature range. The standard treatment to recover the corrosion resistance involves heating the steel to above the dissolution temperature for the carbides and cooling rapidly. The presence of intergranular precipitates is generally indicative of sensitisation in austenitic stainless steels.

By comparison, even rapid quenching is insufficient to prevent carbide precipitation in ferritic stainless steels. Corrosion resistance is restored by heating the material into the

temperature range where the chromium diffusion rate is sufficient to allow chromium diffusion back into the depleted zones, generally referred to as healing. Figure 2 [14] shows the time required for chromium diffusion to the grain boundaries in an 18%Cr steel at various temperatures and provides a clear indication of why healing by chromium diffusion doesn't occur at lower temperatures. The healing operation for ferritic stainless steels makes no attempt to redissolve the precipitates (as in γ steels) and hence the presence of substantial grain boundary precipitates in ferritic stainless steels is no indication of sensitisation.

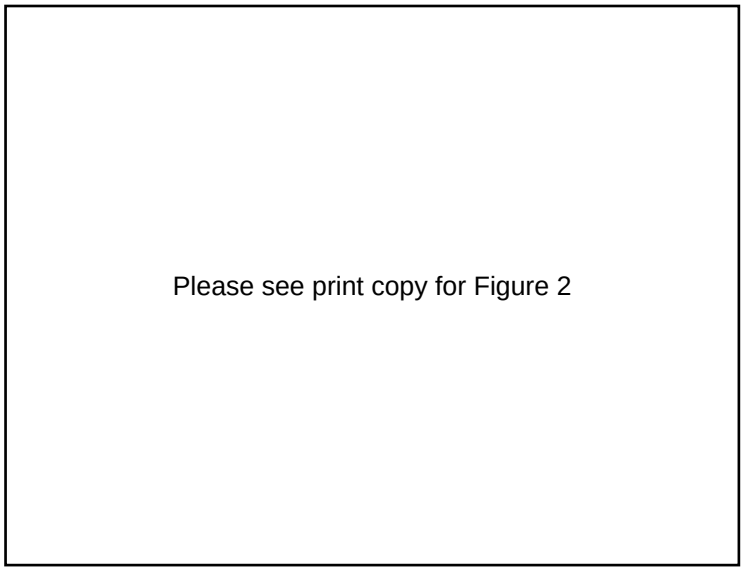

Figure 2 : Calculated Cr Content At Grain Boundary For 18.7Cr- 0.01C Ferritic Stainless Steel (After Arai et al [14])

2.1.4 Prevention

Sensitisation will be reduced or eliminated completely by preventing carbide precipitation from removing chromium from solution and thereby creating the chromium depleted zones. Due to the extremely rapid carbon diffusion rate in the body

centred cubic (BCC) matrix, carbide precipitation can generally not be prevented by rapid cooling [12]. Effective prevention can only be achieved by appropriate control of the interstitial elements and three different methods can be used to achieve this result. These methods involve reducing the interstitial content, stabilisation or controlling the ferrite factor. All of these methods will be discussed individually.

2.1.4.1 Reducing Interstitial Content

Effective prevention of sensitisation in austenitic stainless steels is readily achieved by reducing the carbon concentration to below 0.03% [12] and theoretically a similar approach should be applicable to ferritic stainless steels. However, due to the rapid precipitation rate in the BCC matrix and the low solubility for carbon and nitrogen in ferrite, precipitation cannot be completely avoided. Demo [20] studied the [C+N] levels that could be tolerated in several ferritic stainless steels with varying chromium content, while maintaining adequate corrosion resistance and ductility in the welded structure. He reported that higher levels of interstitial elements could be tolerated with increasing chromium content while maintaining immunity to IGC. The maximum allowable [C+N] in steels with 19%Cr was 60-80ppm with roughly 250ppm being permissible at 35%Cr. Extrapolating from this data, 12%Cr steels would require [C+N] significantly below 60ppm, a target which is not practical for commercial steels.

However, it must be stated that Demo's work was done on steels which were essentially fully ferritic and other researchers [21] have shown that steels which contain substantial fractions of martensite are significantly less prone to IGC than fully ferritic steels with the same chromium content. In their thermodynamic analysis of sensitisation and precipitation [15], Arai et al discuss the anomaly that 17%Cr ferritic stainless steels with

lower carbon are more susceptible to sensitisation than similar material with higher carbon. Based on calculated equilibrium phase diagrams, the authors show that low carbon material (roughly 0.03%) will remain ferritic throughout the heating range while material with higher carbon (0.07%) will form about 10% austenite which will absorb the excess carbon rejected by the ferrite. On cooling, austenite formation on existing γ grains is thermodynamically more favourable than carbide precipitation and subsequently the remaining ferrite is very low in interstitial carbon. However, the γ potential of low carbon steels can be increased by adding alternative γ stabilisers like nickel or manganese and subsequently low carbon would again be preferable in order to prevent sensitisation. While the presence of a small percentage of γ may be beneficial in reducing sensitisation, the mechanical properties (specifically toughness) could be adversely affected by the high carbon martensite which would form on cooling.

Therefore, while very low levels of C and N in ferritic stainless steels will reduce the susceptibility to sensitisation, this does not present a practical method of eliminating the risk of sensitisation in fully ferritic stainless steels.

2.1.4.2 Stabilisation

Stabilisation refers to the addition of alloying elements which preferentially form carbides or nitrides which are more stable than chromium carbo-nitrides. From a purely thermodynamic perspective, possible candidates include titanium, niobium, vanadium, zirconium and tantalum [22]. Ogwu et al. [23] have suggested that combinations of scandium and yttrium with titanium would, again from a purely thermodynamic perspective, be highly beneficial but, given the cost of these elements, they are unlikely to find much practical use in the near future. Tantalum is also too expensive for general

use and vanadium isn't effective in preventing sensitisation due to the sluggish vanadium carbo-nitride precipitation reaction [22] and the fact that the dissolution temperature for vanadium carbides is relatively low at roughly 800°C. To all practical purposes, stabilisation is achieved using titanium or niobium, or combinations of both. Due to its relative abundance and lower cost, titanium is the most generally used element for stabilisation but it does have some disadvantages. These include reduction in toughness and ductility due to presence of large cubic precipitates and solid solution hardening and poor surface finish of the steel sheet during production [22]. Titanium stabilisation is also unsuitable in materials intended for use in highly oxidising conditions where the titanium precipitates are directly attacked and create the appearance of sensitisation. Niobium stabilisation can overcome some of the shortcomings of titanium stabilisation but niobium is less effective as a stabilising agent with the precipitates forming at lower temperatures.

Effective stabilisation depends on a reasonable knowledge of the quantity of carbon and nitrogen in solution so that sufficient Ti/Nb can be added without excessive overstabilisation. Large quantities of titanium in excess of the stoichiometric requirement for stabilisation are known to lead to surface defects in the strip [24]. Several formulas have been proposed for the minimum amounts of stabilising element required in order to assure complete immunity to intergranular corrosion (IGC). Dundas and Bond [25] proposed that the minimum titanium should satisfy the formula

$$Ti = 0.2\% + 4*(C+N). \qquad (1)$$

This formula was obtained from experiments using 18%Cr-2%Mo and 26%Cr-1%Mo alloys and the authors do not claim that it is valid for all Fe-Cr alloys. However, their work showed that the simple stoichiometric ratio of Ti/(C+N) was insufficient for adequate stabilisation and a minimum value of 0.2% was determined empirically. While investigating several failures in AISI 409 type exhaust tubes, Fritz and Franson [24] declared that the ASTM A240 specification for stabilisation of T409 was insufficient. The existing specification allowed for 0.08% C, 10.5 – 11.75 % Cr and up to 0.75% Ti with the minimum stabilisation formula given as

$$Ti > 6^* C. \qquad (2)$$

On concluding their investigation, the proposal was made that nitrogen be included in the stabilisation formula and that the minimum stabilisation requirements should be stated as

$$(Ti + Nb) = 0.08\% + 8^*(C+N). \qquad (3)$$

Contrary to these recommendations, Devine and Ritter [26] maintained that the sensitisation resistance was dictated solely by the carbon concentration and was independent of the nitrogen or [C+N] concentration. They showed results where alloys with very similar stabilisation ratios [Ti / (C+N)] suffered IGC if the carbon fraction is high but remained immune if carbon was low and nitrogen high. Dundas and Bond [25] maintained that if the carbon and nitrogen fractions are similar, the effect on IGC corrosion is equal. Logically chromium nitrides will consume chromium from the matrix and therefore chromium depletion could be partially attributable to the nitrogen

concentration. However, due to the lower chromium content in nitrides compared to chromium carbides, the effect of carbon should be stronger. In addition, since nitrides tend to form at higher temperatures than carbides [22] and can be consumed by any residual aluminium or vanadium without detrimental effects, the effect of nitrogen should be less severe than that of carbon.

Sensitisation is however still possible in properly stabilised alloys, specifically at extremely rapid cooling rates. This can be minimised by overstabilisation but large excess quantities of titanium over the stoichiometric requirements are known to lead to surface defects in the steel and are therefore undesirable. The fact that stabilised alloys can still be susceptible to sensitisation and IGC has only recently been reported [27] and the mechanism (dubbed Mode 3) will be discussed in detail later.

2.1.4.3 Controlling The Ferrite Factor

The Kaltenhauser Ferrite Factor (KFF) was derived to determine the tendency for martensite formation in weld metal [10]. It is defined as

$$KFF = [Cr + 6Si + 8Ti + 4Mo + 2Al + 4Nb] – [2Mn + 4Ni + 40(C+N)] \quad (4)$$

Some results of actual HAZ martensite vs. the KFF are illustrated in Figure 3 [28]. While extensive scatter is evident, reasonable correlation between the KFF and the martensite content of weld heat affected zones can be seen.

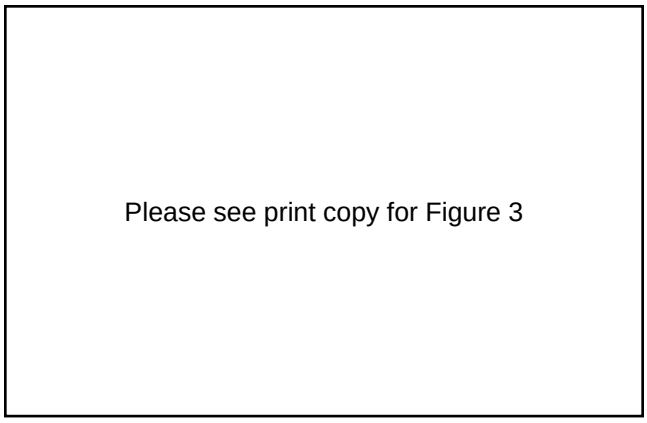

Figure 3 : Influence of Steel Ferrite Factor on HAZ Martensite Content [Gooch et al] [28]

Specifically, a low KFF below 7.5 indicates that ferrite formation is negligible, while high values above 9.5 indicate that substantial ferrite will be retained. At the time when the KFF was proposed, the presence of martensite in the weld was considered detrimental since the presence of hard untempered martensite would reduce the ductility of the weld and could act as stress raisers and crack initiation points.

However, one of the problems plaguing ferritic stainless steels is rapid grain growth at high temperatures [7, 8, 29, 30] with subsequent brittleness, and substantial transformation to austenite and martensite during cooling will result in significant grain refinement and improvement in toughness. More recent developments of utility ferritics have aimed at reducing the ferrite factor in order to increase the austenite potential and thereby maximise the martensite formed on cooling [32]. This can be done quite readily by increasing the carbon content but this is counterproductive since hard, high carbon martensite needs to be tempered to restore toughness and ductility, and this is a major limitation in welding fabrication. By controlling the ferrite factor with other austenite formers (predominantly nickel), a low carbon lath martensite will form during cooling.

Apart from the improved mechanical properties, fully martensitic structures are effectively immune to sensitisation. This is due to the fact that the martensite transformation temperature is below the sensitisation temperature and therefore the structure is still austenite at the critical temperature.

Therefore, by suitable adjustments of the KFF, sensitisation can be dramatically reduced and even eliminated. Lula and Davis [21] reported that of two 17%Cr steels which were investigated, the material which formed 50% austenite at high temperature had considerably less IGC than one which only formed 10% austenite. Sedriks [31] and Marshall [32] maintain that a fully martensitic structure should be immune to IGC because carbon precipitation will occur intragranularly and not on the grain boundaries. As such, the overall corrosion resistance would be reduced but the structural integrity would be maintained.

2.2 Sensitisation In 11-14% Chromium Steels

2.2.1 Metallurgical Overview

The 11-14%Cr steel group is more complex than conventional ferritic or austenitic stainless steels in that small variations in composition, even within the normal allowable variation in steel plant operation, can result in significant variation in properties. The scope for development is also significantly greater because very similar end results by way of mechanical and corrosion properties can be obtained by different methods. Marshall and Farrar published a detailed review [32] of developments in various grades of ferritic/martensitic stainless steels. This review separated 11-14%Cr steels into 4 categories, namely the utility ferritics, lean martensitics, soft martensitics and new supermartensitics. The last three are categorised by decreasing carbon content and

increasing nickel and molybdenum content in the supermartensitics. Despite the growing interest in these grades, further discussion will be limited to the utility ferritics, which will include grades such as AISI 409, AISI 410S and DIN 1.4003 type alloys, of which 3CR12 is only one proprietary brand.

Predicting the behaviour of 3CR12 on cooling from high temperatures is complicated by the presence of the so-called gamma loop in the typical Fe-Cr phase diagram, depicted in Figure 4 [11]. The position of the gamma loop is strongly dependant on the presence of any impurities. Demo [7] reported that in high purity Fe-Cr systems the gamma loop extends as far as roughly 11.8%Cr. Low levels of impurities extend the gamma loop and dual phase region to between 13 – 14% Cr, as illustrated in the phase diagram by Folkhard in Figure 4, after which the structure is fully ferritic at all temperatures.

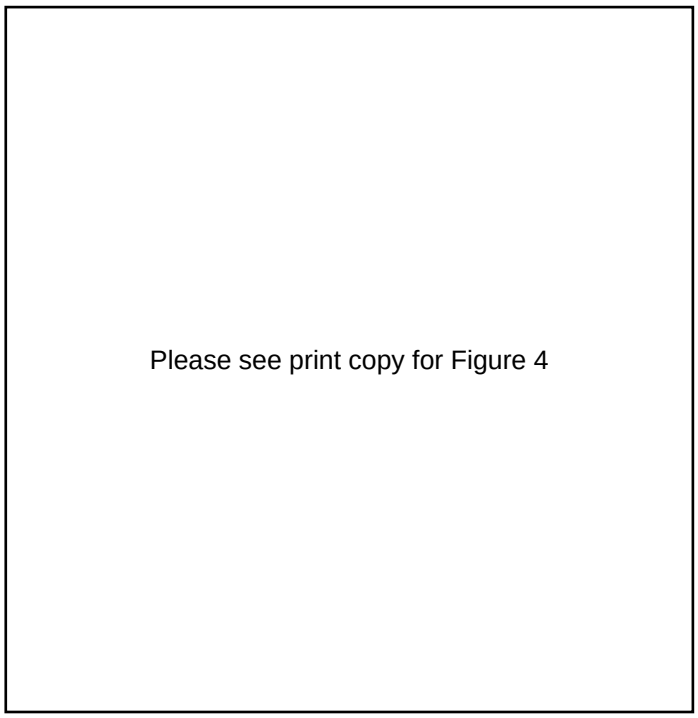

Figure 4 : Typical Fe-Cr Phase Diagram Illustrating The Position Of The Gamma Loop [11].

Several researchers [7, 32] have reported that with increasing carbon and nitrogen, the gamma loop can be extended to as high as 26%Cr, as illustrated in Figure 5. This effect will also be achieved with other austenite stabilisers like nickel and manganese, which is exploited in the development of modern martensitic steels. However, due to the low alloying content, 3CR12 tends to lie in the dual phase region. The structure will therefore consist of a mixture of δ ferrite, α ferrite and martensite, depending on the cooling rate.

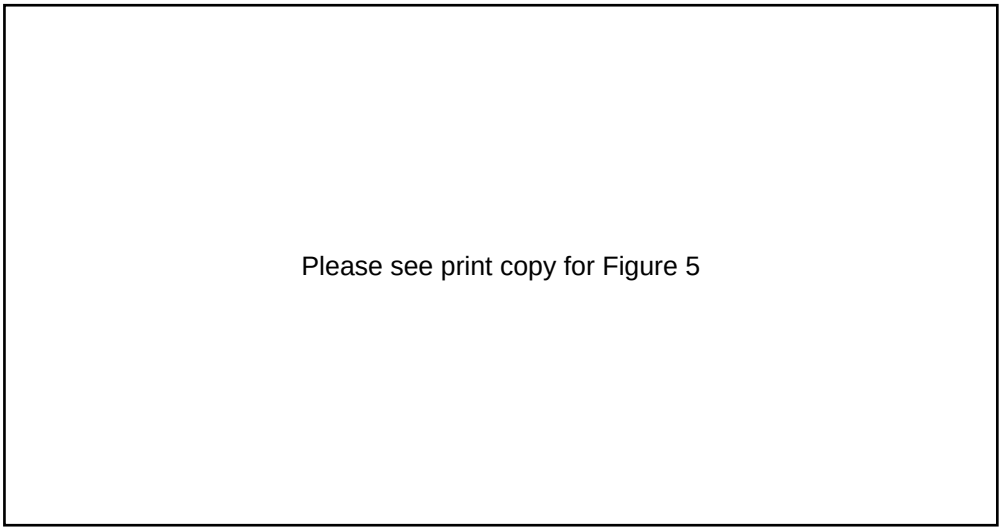

Figure 5 : Shifting Of The Boundary Line (γ + α)/ α In The Fe-Cr System Through Increasing Additions Of Carbon Or Nitrogen [7]

Fully austenitic steels will therefore have 4 distinct transformation temperatures. When referring to the various transformation temperatures, (Ac_1 etc.), the literature is not always consistent. In order to avoid any confusion as to terminology, the following conventions will be used throughout. During any heating cycle the temperature at which ferrite begins to transform to austenite is the Ac_1 temperature. If the alloy composition is such and the steel becomes fully austenitic, the temperature at which the

transformation to γ is complete will be referred to as the Ac_3 temperature. The temperature at which γ starts to transform to δ is then the Ac_4 and the temperature when the transformation to δ is complete is the Ac_5 temperature. The position of these transformation temperatures for an alloy with composition X is indicated on the Fe-Cr phase diagram in Figure 6.

In typical 3CR12 type material, which does not pass into the fully austenitic region, the Ac_3 and Ac_4 temperatures are absent but some reports refer to the upper transformation temperature as Ac_3 [33] while others [34] use Ac_5. This could easily lead to confusion about the nature of the transformation occurring at the Ac_3 temperature unless the composition and position on the phase diagram is clearly specified. To ensure clarity, Ac_3 will be used throughout to indicate the temperature at which the $\alpha - \gamma$ transformation is complete and Ac_5 will refer to the $\gamma - \delta$ transformation.

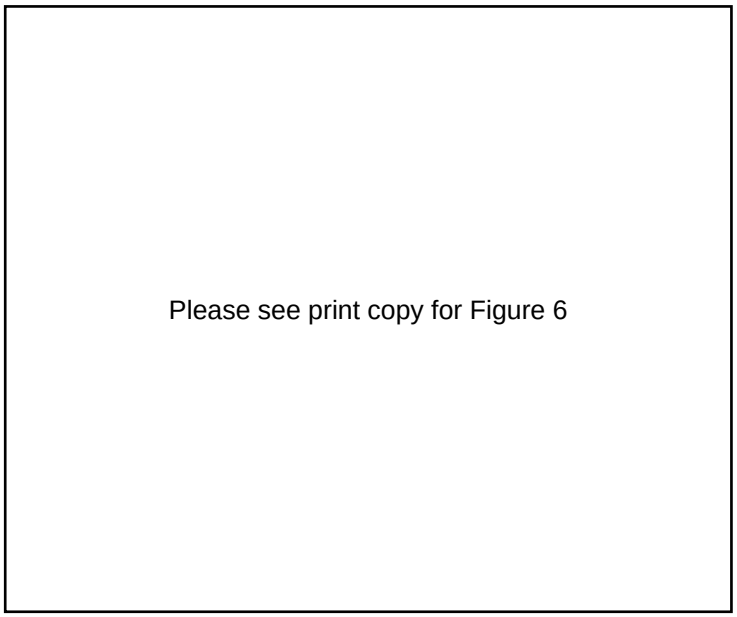

Figure 6 : Positions of Transformation Temperatures on Fe-Cr Phase Diagram after Folkhard [11].

The distinction between α ferrite and δ ferrite is also not obvious when referring to the phase diagram. Figure 6 indicates regions for α, δ and a mixed α+δ region but under true equilibrium conditions it would be practically impossible to distinguish between α and δ. In practice, significant differences can exist between α and δ ferrite. The primary solidification phase is always δ and at the Ar_5 temperature, some δ will transform to γ. Assuming near-equilibrium cooling, all the γ formed will transform to α at the Ar_1 temperature. Simplistically, α ferrite is therefore formed by transformation from austenite while δ does not undergo any transformation on cooling. Under equilibrium conditions, the difference between α and δ ferrite would be insignificant but Knutsen [35] has shown that (under non equilibrium conditions) significant partitioning can occur between the δ and γ, with the austenite stabilisers (carbon, nitrogen, nickel) segregating to the austenite and the ferrite stabilisers (chromium, molybdenum) segregating into the ferrite. This has been shown to occur extensively with long holding times in the duplex region (±1000°C), typically during hot rolling. Differences as high as 2% were reported in the chromium concentration in the δ phase compared to the α/martensite, since it is irrelevant whether the γ transforms to α or martensite. Due to the enrichment of ferrite stabilisers in the δ ferrite, the tendency to transform to γ is dramatically reduced. As a result, during any heating cycle, the α ferrite (or martensite) will transform to γ on heating while the δ grains may remain untransformed, which can result in significant δ grain growth. This segregation effect was also reported by Williams et al [27] and, based on atom probe analysis of the two phases, showed that significantly different Ac_1 temperatures would be expected for the martensite and δ ferrite. Gooch [12] however maintained that no segregation or partitioning was

observed during their work but this referred to welding conditions involving rapid cooling. This would indicate that segregation is certainly possible as described by Knutsen and Williams when extensive hot work is carried out in the dual phase region but significant segregation will not occur during the rapid transformation experienced during welding. Knutsen also maintains that this effect is irreversible and thus α and δ cannot be used interchangeably.

The phase diagram naturally doesn't provide a good indication of the structure which will be found in the Heat Affected Zone (HAZ) of a weld but in conjunction with the typical continuous cooling transformation (CCT) diagram developed by Pistorius et al [34] specifically for 3CR12 (Figure 7), the distinctive features of the HAZ of 3CR12 type steels are readily explained.

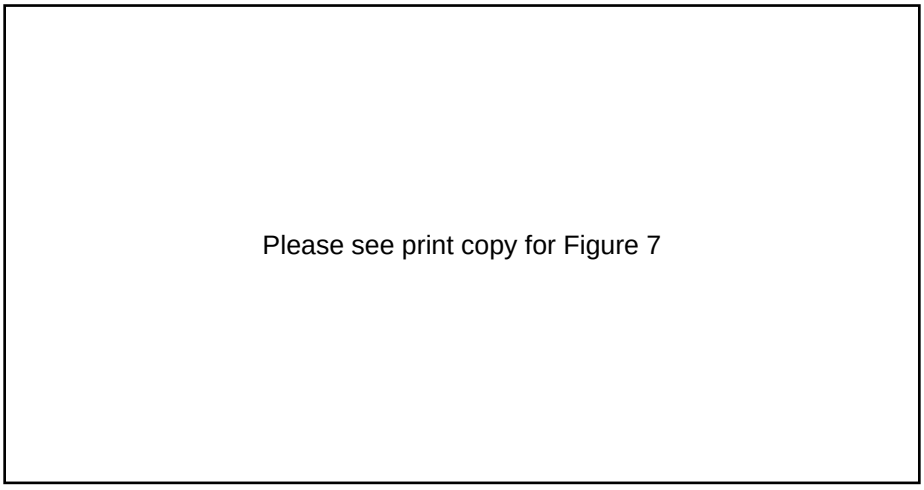

Figure 7 : Proposed Continuous Cooling Transformation Diagram For The Transformation Of δ-Ferrite To γ In The High Temperature Heat Affected Zone During The Weld Thermal Cycle [34]

Unlike the HAZ for plain carbon steels, the HAZ for 3CR12 has 2 visually distinct zones; the high temperature (or coarse grained) HAZ (HTHAZ) and the low temperature HAZ (LTHAZ). This can be explained as follows. Material heated close to the liquidus (above the Ac_5) transforms completely to δ ferrite and rapid grain growth occurs. On cooling, the amount of reversion to γ will be determined by the CCT diagram and therefore the HTHAZ frequently consists of coarse-grained δ ferrite with islands of martensite at the grain boundaries.

The CCT diagram indicates that if the material temperature reaches 1050°C within 1-2 seconds, no reversion to γ will occur and the δ ferrite structure will be maintained to room temperature. Material that cools less rapidly will pass through the dual phase δ/γ region and have a mixed δ-ferrite/martensite structure, typical of the HTHAZ. However, material further from the fusion line, which has been heated above the Ac_1 but below the Ac_5, will contain significant fractions of γ which will transform to martensite, resulting in the tough fine-grained structure of the LTHAZ.

With normal arc welding practice, the amount of ferrite retained on cooling is determined largely by the material composition. As mentioned previously, the most commonly used empirical relationship to determine the tendency of an alloy to form ferrite is the Kaltenhauser Ferrite Factor. More recent work has improved on this by using the Schaeffler approach to produce a constitution diagram using the Kaltenhauser element coefficients. This produces the diagram as shown in Figure 8 [28].

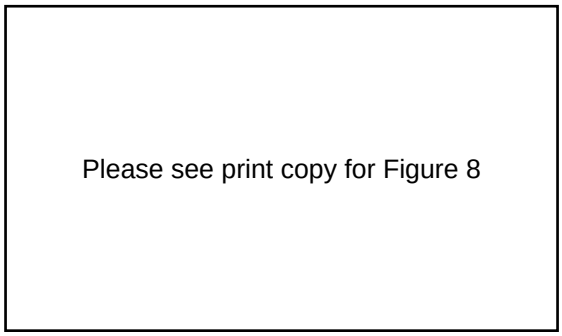

Figure 8 : Constitution Diagram For 12-18% Cr Steel Weld Metals [28]

This diagram is applicable for material with up to 18%Cr and roughly 0.4%Ni and is not applicable to newer alloy designs with higher levels of nickel and molybdenum. The results produced by Irvine et al [3] prompted Gooch [28] to propose a modified constitution diagram with significantly different coefficients for silicon and titanium, as shown in Figure 9.

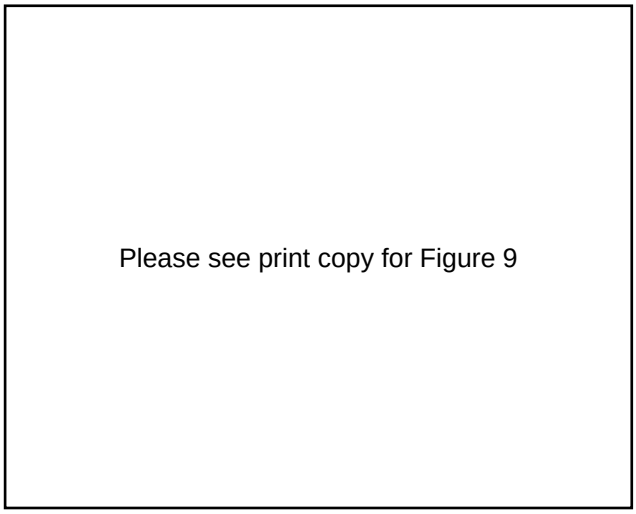

Figure 9 : Preliminary Constitution Diagram For Arc Weld HAZ In Low Carbon 13% Cr Steels [28]

2.2.2 Modes Of Sensitisation

Extensive work by Williams and Barbaro [27] has shown that the origin of sensitisation, i.e. the creation of chromium depleted zones, can be ascribed to 4 different processes or modes. These modes distinguish between where and how the chromium depleted zone will be formed and the thermal conditions required to create the chromium depletion. These modes will be discussed in detail below.

2.2.2.1 Mode 1

This mode of sensitisation is linked to the presence of untempered martensite in the steel before it is exposed to the sensitising temperature. This means that as a result of a single weld pass, sensitisation can occur parallel to the weld bead wherever the material reached the critical sensitising temperature. In practice, the presence of substantial amounts of untempered martensite in 3CR12 sheet will only occur if the material was incorrectly annealed i.e. the Ac_1 temperature was exceeded during annealing or any form of heat treatment before processing. Mode 1 is potentially the most severe manifestation of sensitisation in these steels, principally because it is likely to extend over a large area. If a plate or edge of a coil is overheated during the final annealing stage, it renders the entire area susceptible to sensitisation if it is welded. The sensitised region can therefore be very widespread and extend along the entire length of a weld bead. However, commercially available material should not contain any untempered martensite since the material is not deliberately heated above the Ac_1 during annealing.

2.2.2.2 Mode 2

Fundamentally, the mechanism for mode 2 is identical to mode 1, but the difference lies in how the untempered martensite in the material is created. Mode 2 assumes at least 2 welding passes where the first pass created untempered martensite in the HAZ and the critical sensitising isotherm from the second pass causes carbide precipitation in the first HAZ. Essentially both modes require two exposures to high temperature but the manifestation will be different. In mode 1 the intergranular attack will be associated directly with the weld bead that caused the precipitation while in mode 2, corrosive attack will be associated with weld 1 while the precipitation was effectively caused by weld 2. Depending on the weld geometry and dimensions, mode 2 sensitisation can manifest itself on the opposite side of a plate from where the weld was positioned, as illustrated in Figure 10.

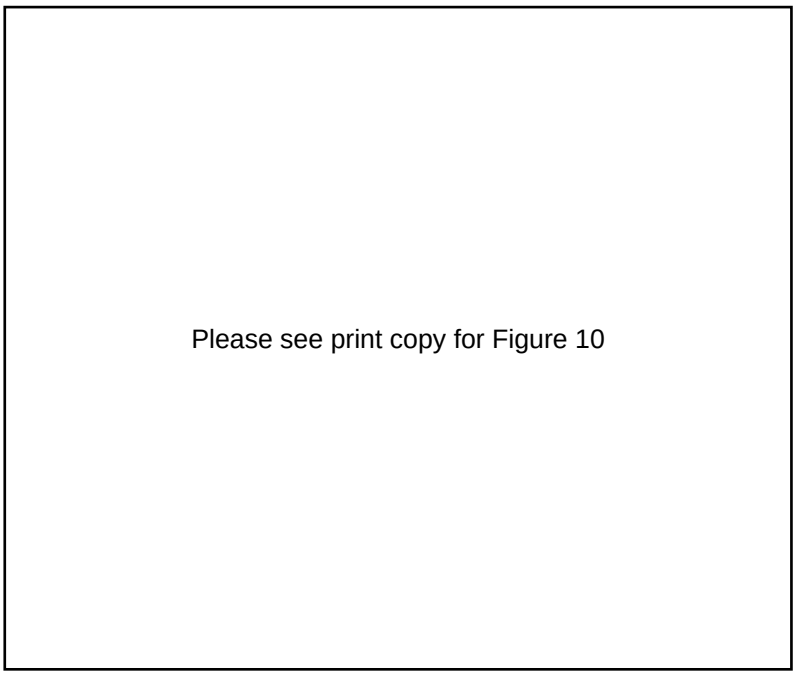

Figure 10 : Influence Of Weld Geometry And Welding Sequence On Mode 2 Sensitisation [27]

It has been shown by Williams [27] and Matthews [36] that the joint configuration and positioning of the weld beads can significantly affect whether sensitisation occurs. If the sensitising isotherm from the second weld only intersects with the filler metal or unaffected base metal, sensitisation is avoided.

Practically speaking, no distinction should be made between mode 1 and mode 2. The two modes were separately identified and given different names in order to distinguish between problems being experienced in service, but the mechanism remains the same. Mode 1 presumes that martensite is present in the structure due to heating above the Ac_1 temperature during annealing or processing. This will never be done deliberately since the presence of untempered martensite in the structure is likely to increase the hardness and tensile strength in excess of the material requirements [37]. 3CR12 type steels are generally supplied in a fully tempered and softened condition and the presence of any untempered martensite in the material is undesirable. As such, mode 1 represents a material processing defect rather than an inherent material property.

2.2.2.3 Mode 3

Mode 3 sensitisation occurs in the HTHAZ (i.e. the coarse grained region adjacent to the fusion line) in material where the HTHAZ is predominantly ferritic. Since the material close to the fusion zone is heated well above the Ac_5 temperature, this mode of sensitisation is independent of any previous heat treatment and material condition. Unlike mode 2 sensitisation, mode 3 occurs after a single exposure to high temperatures above the Ac_5 temperature and has been shown to occur in titanium stabilised steels with higher ferrite factors as well.

This mode of sensitisation isn't very well understood but recent work has shown that it is caused by extremely rapid cooling rates generally associated with very low heat input welds [38] and by shallow weld toe cusps and arc strikes [27]. As can be seen from the CCT diagram for 12%Cr steels [34], very rapid cooling from above 1350°C will result in a fully δ ferrite structure. At these elevated temperatures, even TiC and TiN can dissolve to release carbon and nitrogen back into the δ matrix. If the γ transformation is suppressed during cooling, there will be a strong tendency for carbides to precipitate to the grain boundaries as the material passes through the critical temperature range. It appears that reformation of Ti(C,N) precipitates is kinetically unfavourable under these conditions and preventing sensitisation is therefore achieved by the presence of sufficient γ during cooling which absorbs and traps the carbon and nitrogen rejected by the δ ferrite during cooling. In the recent work by Greef and du Toit [38], it was shown that for equal heat input levels, material with a higher γ potential had a lower propensity for sensitisation than material with lower γ potential. It was also shown that increasing the heat input resulted in reduced sensitisation due to lower cooling rates which resulted in more δ reverting to γ. This work confirms previous reports by Gooch et al [28] that the degree of sensitisation in single pass welds would depend on the phase balance of the material. Similarly, Miyakusu [39] proposed that the risk of IGC would be eliminated when the following criterion is met :

$$\%C < (0.0028 * \%\ \text{Martensite}) - 0.013 \qquad (5)$$

This formula was derived for ferritic 17%Cr-Ni steel and applying this formula to the results obtained by Greef and du Toit [38] does not give very good correlation. The

carbon in the material used in this work was 0.018% and 0.012% and at these carbon levels, anything above 12% martensite should have suppressed IGC. However, the results show that sensitisation was only effectively eliminated when the martensite percentage was greater than 25%.

It is therefore desirable to increase the level of austenite reformation during cooling in order to maximise the volume of martensite in the HAZ. Gooch [40] suggested that preheating in the region of 300°C would result in slower cooling with a subsequent increase in the volume of γ formed on cooling, but also commented that very little success had been achieved. Even if moderate success had been observed, this would not necessarily represent a practical solution because it negates the benefits that the utility ferritics were designed to deliver, specifically ease of fabrication, similar to that of carbon steels. Meyer et al [41] investigated the possibility of using high carbon electrodes or an Ar/N shielding gas mixture to increase the austenite potential of the HAZ. While the investigation was focused on decreasing the ferrite grain size by increasing the grain boundary martensite in order to improve the toughness, a larger volume fraction of austenite would assist in preventing sensitisation as well. The test results showed that finer δ grain size could be obtained together with increased grain boundary martensite, but the high carbon filler metal resulted in a significantly harder HAZ and introducing sufficient nitrogen into the shielding gas resulted in excessive spatter.

Disregarding cooling rate effects, the amount of ferrite retained in the HTHAZ will be determined by the alloy composition. As indicated previously, KFF values above 9.5 indicate that extensive amounts of ferrite will be formed while for values below 8 the

structure would be fully martensitic. While it is fairly safe to say that material with a KFF above 9.5 is likely to be prone to mode 3 sensitisation, it is not possible to make such predictions for material with the KFF in the range between 8 and 9.5 (see Figure 3 and Figure 11). Using the element coefficients proposed by Gooch [28] in the creation of the modified constitution diagram (Figure 8), Williams et al [27] proposed a modified ferrite factor (FF_{BSL}) as follows

$$FF_{BSL} = [Cr + 3Si + 16Ti + Mo + 2Al + 2Nb] – [2Mn +4Ni + 40(C+N) + 4Cu] \quad (6)$$

Using this modified formula, Williams reported that sensitisation behaviour could be predicted more accurately, with FF_{BSL} below 8.5 being immune to mode 3 sensitisation.

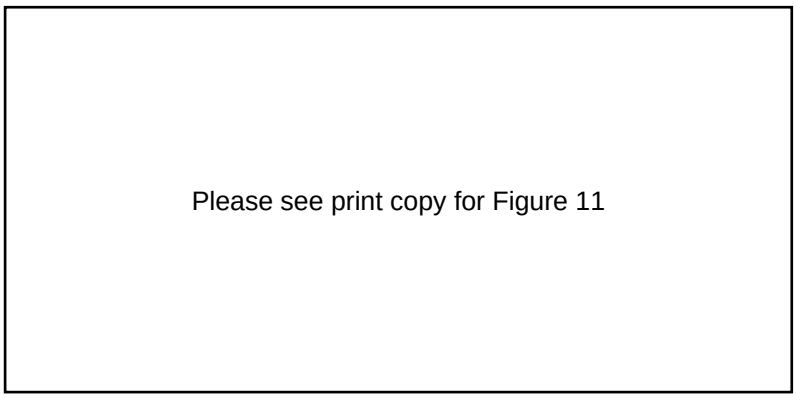

Figure 11 : Effect Of Ferrite Factor On Performance In IGC Test For Mode 3 Sensitisation [27]

It is important to note that the mechanism of sensitisation in modes 1 and 2 is significantly different from mode 3, in that for modes 1 and 2, the martensite phase is sensitised while in mode 3, sensitisation occurs in the δ ferrite. However, it has been reported [21] that high carbon steels like AISI 410 which are fully martensitic do not sensitise after welding. Other authors [32, 39] maintain that a minimum threshold level

of martensite is desirable. Marshall [32] states that martensite introduces intergranular boundaries which are highly favourable for carbide precipitation. However, the presence of martensite increases the phase boundary area due to the inherently fine grain size and due to carbon partitioning into the γ (and hence martensite), less carbon will be available to precipitate elsewhere in the microstructure. Carbide precipitation occurs on lath boundaries within the martensite, reducing general corrosion resistance but is not expected to produce typical sensitisation. Nevertheless, in the same study done together with AISI 410 steels, Lula [21] reported that AISI 405 type steels, which had a dual phase microstructure, were sensitised. The work done by Matthews et al [33, 36] was also done on dual phase steel and it appears that the presence of some ferrite is required for sensitisation to occur.

2.2.2.4 Mode 4

Mode 4 sensitisation is only associated with steels which have a relatively high Ac_1 temperature. The Ac_1 for common 12%Cr steels ranges between 760°C and as high as 840°C. The mechanism for mode 4 has not been confirmed but it is believed that carbides start to dissolve in the region just below the Ac_1 and then precipitate as chromium carbides on cooling. The model proposed by Williams [27] suggests that elements such as boron and vanadium are involved. It is suggested that chromium borides and vanadium carbides dissolve at temperatures around 800°C and then chromium carbides precipitate on cooling. In their review on stabilisation and potential carbide forming elements, Gordon et al [22] report that vanadium is unsuitable because of sluggish precipitation and because VC dissolves close to 800°C, which correlates with the hypothesis by Williams. Vanadium was present as a residual in all the materials showing mode 4 in the work done by Williams et al [27] and, if the resulting

sensitisation is due to VC dissolution, this would explain the observation that the severity of mode 4 sensitisation is generally low. Williams also suggests that some dissolution of carbo-nitrides can start occurring from temperatures above 790° since the solubility limit of carbon at this temperature can be as high as 0.03% [11]. In steels with low Ac_1 temperatures, any dissolved carbon or nitrogen will be absorbed by the austenite formed when the Ac_1 temperature is exceeded. The severity of mode 4 is therefore strongly dependant on the amount of carbon and nitrogen released into solution and the temperature range between the dissolution temperature and the Ac_1. The severity of mode 4 would be expected to increase with higher heat input and resultant increased time at the dissolution temperature. Conversely, very low heat input and fast travel speeds have been shown to be instrumental in causing mode 3 sensitisation [38] and therefore the heat input needs to be controlled within an optimal range.

Mode 4 can occur after a single heat cycle and is not dependant on martensite being present or created by previous heat cycles. A third zone has therefore been identified in the HAZ and is generally referred to as the subcritical HAZ [36]. This area was previously considered as being unaffected by welding cycles since no phase transformations occur but with the isolation of mode 4 sensitisation, this region becomes highly significant, especially since it is practically impossible to distinguish it visually from the LTHAZ.

2.3 3CR12 Production And Processing

As shown in the previous section, sensitisation in 3CR12 type alloys can be avoided by titanium stabilisation and by designing an alloy with a low ferrite factor. While

extremely simple in theory, this represents some problems for the manufacturer to maintain the advantages that the utility ferritics were originally designed for. Since titanium is a very strong ferrite stabiliser, the presence of titanium needs to be offset by appropriate amounts of γ stabilisers, but the two most potent candidates (carbon and nitrogen) are undesirable. This leaves manganese and nickel as suitable candidates and these elements are typically added in concentrations of roughly 2% and 1% respectively. With these concentrations a fully martensitic HTHAZ can be achieved which has the additional advantage of having increased toughness, since the presence of coarse δ ferrite is eliminated. This does however present a major challenge to the steel maker because both these elements depress the Ac_1 temperature and increase the tempering resistance of the steel [7]. High Ac_1 temperatures are advantageous because they allow higher annealing temperatures, which decreases the required holding time and increases throughput, resulting in lower cost. Steels with low Ac_1 temperatures require batch annealing which is a slower process compared to continuous line annealing, which is possible with higher Ac_1 temperatures.

However, these options do not provide a solution in all circumstances. In comparison to fully ferritic grades like 409 and 430, 3CR12 is considered to have good weldability and HAZ toughness in thick as well as thinner gauges and is supplied in thicknesses up to 30mm [37]. Material 10mm and greater is most commonly supplied as shear plate and not as coil, i.e. the final flat strip is cut directly to the desired length after hot rolling without being coiled. With the relatively high cooling rates experienced during the cutting process, complete transformation to martensite will take place, irrespective of the Ac_1 and chemical composition. Annealing is therefore required but an equivalent of batch annealing for stacks of cut plate becomes impractical and expensive. As a result,

titanium stabilised material in gauges above 8mm is generally not available and unstabilised material is still being imported into Australia.

Unstabilised thick gauge material is theoretically highly prone to sensitisation. Since the work by Williams [27] and Matthews et al [33, 36] showed that intersecting isotherms can lead to sensitisation, thick gauge material, which requires multiple passes for the simplest joins, will naturally have several overlapping weld beads with overlapping and intersecting isotherms. It is not a foregone conclusion that critical sensitisation will take place since the position of the beads and the degree of overlap will determine whether any particular HAZ is sensitised by subsequent weld beads. The work by Matthews et al [33] also showed to what extent the degree of overlap influenced the presence of sensitisation and IGC. A significant factor is also whether the sensitised region reaches the surface of the plate or whether it remains within the interior where it is innocuous.

2.4 Detection Methods For Sensitisation

2.4.1 Immersion Testing Methods

Several methods have been determined for detecting sensitisation and these are defined in the ASTM standards A262 and A763 for austenitic and ferritic stainless steels respectively [42, 43]. Since these tests were originally intended for assessing steels of significantly higher alloying content than 12%Cr, these methods are not directly applicable to the materials being investigated. The least aggressive test given in ASTM A763 requires 24 hours in a 16% H_2SO_4 / copper sulphate solution and is specified for 430 type steels. Apart from the immersion time, this test (ASTM A763 Practice Z) is similar to ASTM A262 Practice E, which is commonly referred to as the "Strauss Test". However, some researchers [44, 45] showed that this test resulted in

extensive general corrosion in low chromium steels and sensitisation could not reliably be detected. After further experimentation with reduced acid concentrations, Devine & Drummond [44] determined that 20 hours in 0.5% H_2SO_4 with elemental copper and copper sulphate appeared to give optimum results. This work was later confirmed by Fritz & Franson [24, 46] and this method has now become the de facto standard for sensitisation testing in low chromium stainless steels.

While the standards call for weight loss measurements or cracking during bending for sensitisation to be confirmed, the most obvious manifestation of corrosion taking place is deposition of elemental copper at the corrosion sites. However, Williams et al [27] showed that IGC could occur without obvious copper deposition on the surface of the test specimen. The presence of intergranular attack was observed microscopically after samples were lightly polished after testing. This was particularly the case with sensitisation caused by the mode 4 mechanism which is believed to be less severe than the other defined modes. However, no evidence has been found that correlates the presence of copper deposition with severity of sensitisation.

2.4.2 Electrochemical Detection Methods

The degree of sensitisation can be determined by weight loss measurements but these techniques are complicated by the deposition of copper on the sample, necessitating complete removal before accurate weight loss can be determined. Quantitative results can therefore more readily be obtained more accurately by electrochemical methods. Pistorius et al [47] used potentiostatic etching to determine whether sensitisation was present in 430 type material. This test involved scanning the sample at a potential where the base material was passive but chromium depleted areas would be in the active

region and hence corrode. The current density during etching provides a quantitative indication of the degree of sensitisation and SEM investigation confirmed that IGC had occurred. However, during further work by Greef and du Toit [38] it was found that this technique was difficult to apply to the HAZ of welded samples because the area of the HAZ could not be determined accurately. The technique did however provide a very useful electrolytic etching technique which showed very clearly where IGC was occurring when the material was examined under a microscope.

The standard ASTM evaluation methods suffer from 2 fundamental flaws, namely that they are relatively slow and the degree of sensitisation cannot readily be quantified. The results may frequently be open to interpretation and Walker [48] reports that in an exercise evaluating ASTM A262 Practice E, in certain cases the same samples were ranked as passed or failed by different organisations. In their evaluation of detection techniques, Clarke et al [49] argue that the degree of sensitisation and the consequences thereof are highly dependant on the application. They maintain that the presence of stress can lead to intergranular stress corrosion cracking in moderately sensitised steels where no appreciable IGC is noted in the absence of stress. Conversely, material might perform satisfactorily in service despite having failed the standard tests for sensitisation and therefore more discerning evaluation techniques are required.

Electrochemical evaluation techniques for IGC have generally found acceptance for austenitic and high chromium ferritic stainless steels [21, 50, 51], but their application to low chromium steels has been limited. This is largely due to the concern that these methods will not be effective on a dual phase microstructure and that preferential attack on martensite will overshadow the response attributable to IGC. Electrochemical

potentiokinetic reactivation (EPR) techniques have been applied successfully to AISI 405 [52] (which generally has a ferrite/martensite structure) and to 410S [53] (which is predominantly martensitic), and the method should therefore be suitable for 3CR12 type steels as well. The test conditions need to be fairly specific due to the relatively low corrosion resistance of 12%Cr steels and the pH and temperature of the test solution need to be controlled within close limits. The test involves applying an anodic scan from the corrosion potential into the passive range and then reversing the scan, as shown in Figure 12 [51].

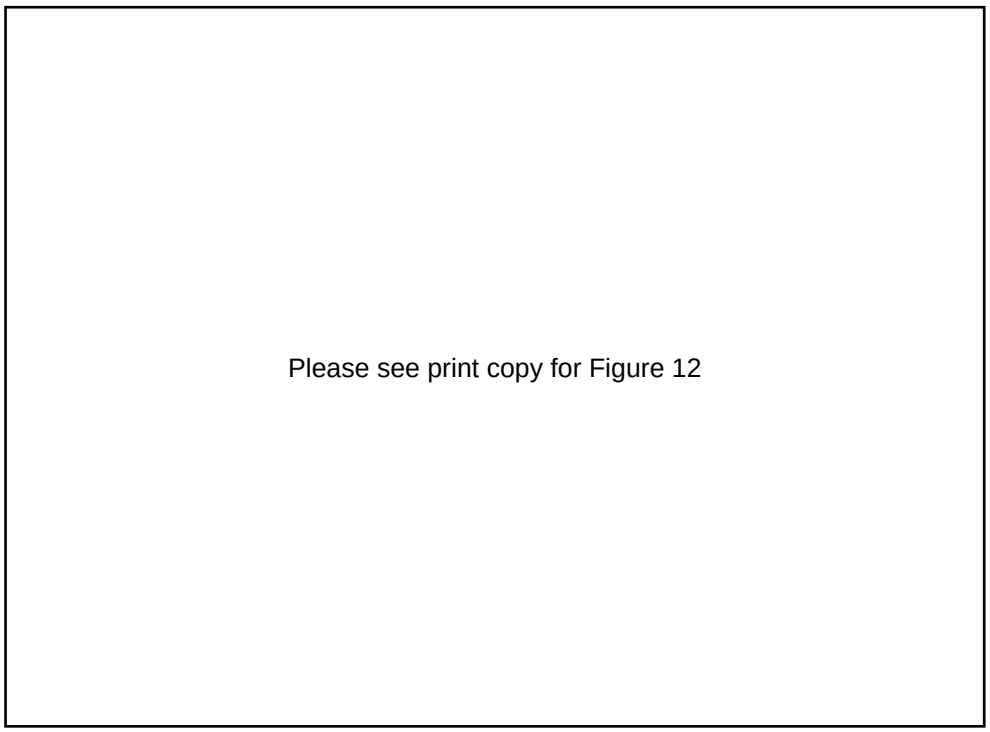

Figure 12 : Schematic Diagram of the Double Loop EPR Test. Evaluation is by the Ratio Ir : Ia [51].

The ratio of the activation current on the anodic scan (Ia) and the reverse scan (Ir) provides an indication of the degree of sensitisation. The detailed theoretical basis for this technique can be found in the article by Majidi and Streicher [51]. When applying the technique to dual phase steels, some authors [52, 53] report that preferential

martensite attack had a strong impact on the shape of the reactivation curve but a quantitative measurement of the degree of sensitisation could still be obtained from the Ir/Ia ratio. The main advantage of this double loop scan technique is that the current does not need to be normalised for the grain size of the specimen.

Vyas and Isaacs [50] also report that the EPR technique is successful in evaluating austenitic stainless steels and that it can be used to determine the degree and position of the sensitised region of the HAZ by successively machining material from a plane parallel to the weld direction and plotting the activation charge as a function of the distance from the weld. This method is obviously extremely time consuming and an alternative method, namely the scanning reference electrochemical technique (SRET) is described. In this technique a microtip reference electrode scans the surface of the sample and measures the potential variations in the electrolyte from the local corroding sites. The degree of sensitisation was clearly indicated by the potential peak height. However, no similar study on ferritic steels has been found.

2.5 Scope Of Work

The proposed study is being undertaken to determine to what extent unstabilised 3CR12 heavy plate material is sensitised by multi pass welding. Intuitively, all of the 3 identified separate modes of sensitisation (with mode 1 being a specialised case of mode 2) could occur in commercially available material. Mode 2 sensitisation will almost certainly be present since long overlapping parallel runs cannot be avoided. Mode 3 is less likely because the standard welding conditions are not conducive to producing the extremely high cooling rates required for mode 3 sensitisation to occur. This mode can

also be prevented most readily by using higher heat input while remaining well within the recommended parameter range. The possibility of mode 4 sensitisation occurring is more difficult to predict since this mode is more dependant on the material composition and on heat to heat variation of the composition than the other modes.

The important questions that need to be considered are therefore as follows.

To what extent does multiple pass welding cause sensitisation of unstabilised heavy gauge 12Cr plate and where does it occur?

Does the introduced sensitisation affect the integrity of the weld?

Is the degree of sensitisation influenced significantly by the welding parameters?

These issues will be addressed in the proposed study.

3 Experimental Procedure

As stated previously, the aim of the work carried out was to determine the extent to which multiple weld passes and the varying heat input influences the degree of sensitisation in thick gauge 3CR12 material. The experimental work carried out can be grouped into 4 sections, namely bead on plate (BOP) welds, straight butt welds, thermo-mechanical simulation and electrochemical evaluation. The material for the investigation was supplied by Atlas Speciality Metals, who import the steel from various suppliers around the world. Material from two different manufacturers was provided and plates from two different batches were also supplied from supplier A. The chemical analysis as supplied on the material test certificate for the material is given in Table 1 below.

Table 1 : Chemical Analysis Of Tested Material (All Values In Wt %)

Mat ID	C	S	P	Mn	Si	Ni	Cr	Mo	Ti	N	Cu	Co
A 1	0.016	0.0005	0.023	0.957	0.247	0.416	12.45	-	0.003	0.0080	-	-
A 2	0.012	0.0016	0.027	0.910	0.280	0.588	12.20	-	0.004	0.0073	-	-
C 1	0.030	0.0040	0.028	0.410	0.640	0.380	11.32	0.02	0.033	0.0140	0.12	0.02

These analysis values have been used to calculate the various material characteristics as given in Table 2 below. As expected, the KFF value is higher than the FF_{BSL} and according to the criteria given by Williams [27], only material A2 should be immune from Mode 3 sensitisation, even though the difference between the analysis of A1 and A2 is normal variation between production casts from the same manufacturer. However, while the prediction for the martensite start transformation temperature is fairly

consistent for the formulas used by Smith and Gooch, the same cannot be said for the Ac_1 temperatures.

Table 2 : Material Characteristics Of The Supplied Plate (Temperatures In °C)

Mat ID	KFF [10]	FF(BSL) [27]	Ac_1 (Folkhard) [11]	Ac_1 (Smith) [54]	HAZ M% (Matthews) [36]	Ms (Smith) [54]	Ms (Gooch) [28]
A 1	9.42	8.70	824.5	765.0	77.8	385.7	376.5
A 2	8.97	8.16	819.9	751.9	80.8	404.3	375.2
C 1	11.40	9.21	797.7	826.4	77.5	431.7	385.5

Given that all the steels are unstabilised, the Ac_1 temperature is an important factor in determining susceptibility to mode 4 sensitisation. The values calculated by Smith et al [54] are determined from an empirical model based on dilatometry results of several hundred analyses and was specifically developed for 12-14%Cr steels, while the Folkhard equation is possibly more limited, and as such the results given by Smith are more likely to be accurate.

All the preliminary work was done using material A1. Material availability from supplier C was limited and hence the initial trial work done to determine the optimal experimental conditions was only done using one grade. Once the experimental difficulties had been overcome, material from both suppliers was welded and tested to obtain comparative results between the two variants. Direct comparisons have only been made between material A2 and C1. The available material from batch A1 was consumed for the preliminary experimentation and additional material had to be obtained for the comparative study. The variation in the analyses of A1 and A2 is typical of the level of variation expected in commercial production and no comparisons between these two materials have been made.

3.1 Bead On Plate Welds

The multiple BOP welds were carried out on flat pieces of 10mm gauge material 50mm wide and 300mm long. The weld bead was laid down along the full length of the sample to ensure that a stable and consistent weld bead could be obtained. The beads were laid down as shown in Figure 13 and the heat input was varied between 0.5 and 1.0 kJ/mm. After five beads had been laid down as illustrated, an additional 2 beads were placed on top of the initial five for half of the sample length. The aim was to determine whether the second layer of weld metal affected the HAZ created by the first layer, specifically whether the coarse grained HAZ would be reduced by being reheated into the dual phase region or whether any tempering of the martensite would occur.

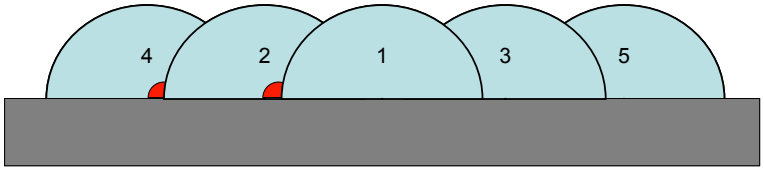

Figure 13 : Schematic Layout For BOP Welds

As per the manufacturer's recommended welding practice, the filler metal used was 1.2mm flux cored type 309 austenitic wire and the shielding gas used was StainShield Lite (Argon, 1% O_2). Shielding gas containing carbon dioxide is not recommended, due to the possibility of carburisation. The sample plates were clamped to a base plate during the duration of the test and restrained until the temperature of the plate had decreased below 100°C. This was done to prevent the pieces from bowing as the weld bead contracted, since this made controlling the contact tip to weld distance impossible. The interpass temperature was controlled to below 60°C and the plate was allowed to cool naturally without forced air or water quenching between passes.

The welding torch was clamped to a Bug-O® system trolley which ran along a rail mounted parallel to the base plate. The travel speed of the trolley could be controlled accurately between 0.20 and 1.0 m/min.

Transverse samples were cut across the welds for metallographical analysis and sensitisation tests. The samples were cut using a band saw so as to prevent any local overheating of the surface and then ground to 1200 grit finish and then polished to a 1μm finish. The additional samples which were to be subjected to the Strauss test were only ground to 800 grit finish. Etching with acidified $FeCl_3$ solution or Kallings No 2 revealed the coarse primary ferrite in the CGHAZ and the martensite/ferrite HAZ and matrix. Electrolytic etching in 10% oxalic acid clearly revealed the regions of fresh untempered martensite where effectively no carbide precipitation had occurred and severely attacked the grain boundaries where precipitation had occurred. This method did not indicate sensitivity to IGC since the entire base metal structure showed similar grain boundary and intragranular attack on the martensite. What the oxalic acid etch did highlight was regions where the HAZ from subsequent beads had tempered the HAZ from previous runs. These tempering effects could be confirmed with hardness traverses across the samples.

3.2 Straight Butt Welds

The butt welds were done joining two pieces of 10x40x300mm flat bars which had a double sided 60° V weld preparation with a 1.5mm landing as shown in Figure 14, as per the manufacturer's recommended practice [37]. The samples were tacked at either end so that a 2mm gap was left at the bottom of the V-notch. Due to the prevalence of

slag inclusions noted in the BOP welds, the filler metal was changed to be 0.9mm solid 309L type wire. The tacked sample was again clamped to prevent bowing but a 10mm gap was left between the sample and the base plate. For the preliminary experiments on material A1, no backing bar was used for the root pass and the back side of the root pass was ground out before the backing pass was laid down. Root penetration was not very good on these initial weld runs and thorough back grinding was done before the back pass was laid down.

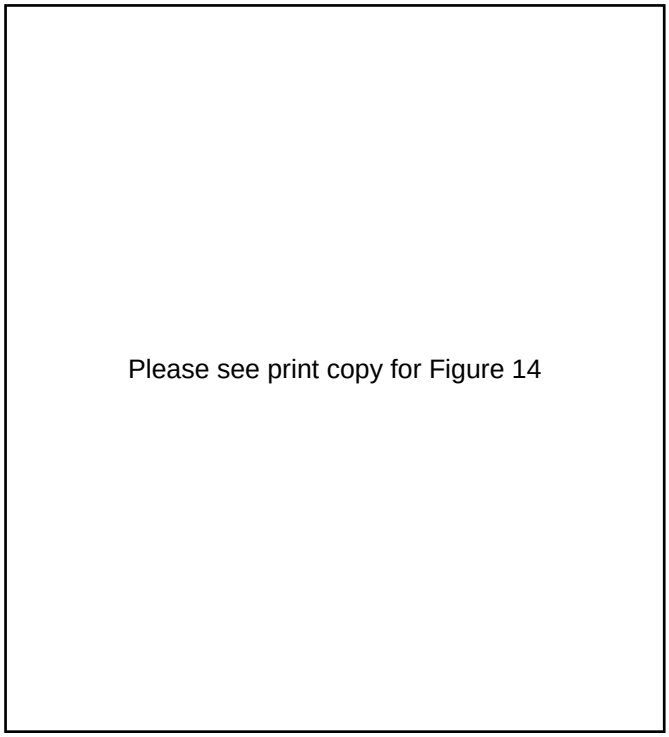

Figure 14 : Recommended Joint Preparation [37]

A ceramic backing strip was used on the later welds using material A2 and C1. Better control of the root pass could be achieved and root penetration was significantly better on these welds. Back grinding was still done on all samples but was less extensive than for material A1. The welds were cleaned with a stainless wire brush between passes but

grinding was only done on the root run. The detailed welding parameters employed are given in Table 4. The back pass was always done as the very last pass in order to simplify the experimental procedure, even though it was contrary to the manufacturer's recommended welding sequence. Preliminary work had shown that the HAZ from beads 4 and 5 (as per Figure 14) was not large enough to interact with the backing pass.

As with the BOP experiments, samples were cut for metallographical examination and sensitisation testing. The sample preparation and etching techniques are the same as used on the BOP samples. All BOP and butt welds were tested using the Strauss test.

3.3 Modified Strauss Test

The modified Strauss test is a variation on ASTM A 763-93 Practice Z [43] for detecting susceptibility to sensitisation in ferritic stainless steels. Samples are placed in a copper sulphate solution (60g $CuSO_4$ in 1l of water) which is acidified by adding 0.5% sulphuric acid (3ml H_2SO_4 in 1l water). A layer of copper shot is placed on the bottom of the vessel and the samples are placed in the solution in such a way as to prevent direct contact with the welded region. The solution is then boiled for 20 hours.

During the test, chromium depleted regions will undergo anodic dissolution and copper will be deposited on the corroding regions. This generally highlights the areas where IGC is occurring but sometimes this can be masked by other corrosion products. Copper will deposit anywhere that corrosion is occurring and if any pitting or crevice corrosion takes place, copper deposition will be seen. The samples, which had been analysed metallographically, as well as two additional samples from every weld, were tested by this method. The polished specimens were placed in the vessel so that the polished

surface was horizontal and facing up while the other specimens were placed so that the weld bead was parallel with the base of the vessel, i.e. the cut surfaces were vertical. After the samples were removed from the test solution, all surfaces were scrubbed with a soft brush to remove any excess copper and other surface accumulation.

If metallographical analysis was required after the samples had been tested, the samples were cleaned in nitric acid to remove the copper and then polished lightly.

3.4 Welding Simulation

The metallographic examination of the results obtained from the welding trials indicated that mode 4 sensitisation represented the greatest problem, but very little difference could be detected in the degree of sensitisation by the Strauss test. Electrochemical methods would be necessary to determine whether variations in the welding parameters produced a significant difference in the sensitisation behaviour. Since the area affected by mode 4 sensitisation is relatively small, it is very difficult to produce samples which only contain material which has been sensitised by mode 4. Thermal simulations were therefore done in order to produce samples where any sensitisation was definitely the result of mode 4.

The thermal treatment was performed on the Gleeble 3500 simulation system. Standard 10mm diameter samples were machined at 118mm length from material A2 and C1. Three thermocouple pairs were spot welded to the sample in the configuration shown in Figure 15. The temperature was controlled by the central thermocouple (TC2). The samples were heated to 800°C at approximately 250°C/s and held at that temperature for 0.5s. The cooling rate was then varied between the maximum obtainable by forced air

quench and the natural cooling rate under vacuum. The cooling rate within the sample could be seen to vary, with the sections closer to the copper contacts cooling more rapidly, as would be expected. Sections were then cut from the samples at the positions where the thermocouples had been attached and where the cooling rate (at least, at the surface of the specimen) was known.

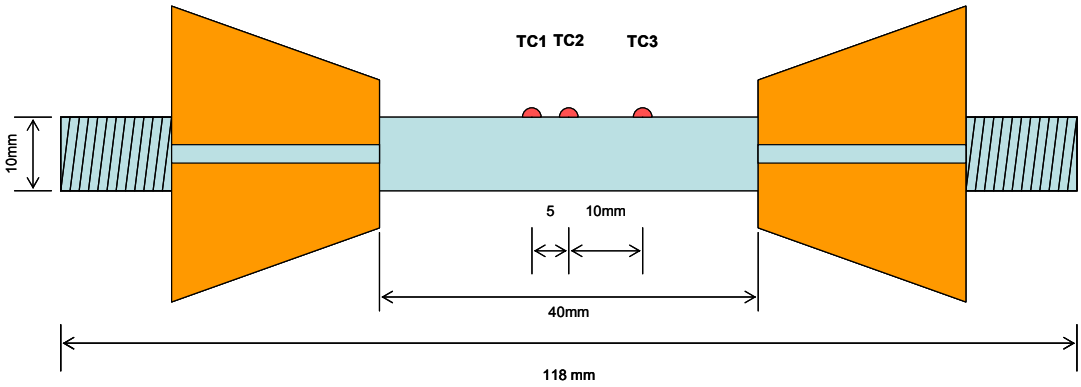

Figure 15 : Schematic Of Gleeble Sample Indicating The Thermocouple Positions And Dimensions

The temperature profiles that were obtained for the various cooling rates are shown in the figures below. It can be seen that the heating rate slows down as the sample temperature approaches the aim temperature. This was done deliberately in the temperature control program after problems were experienced in obtaining a consistent peak temperature. Initially the control program was set to heat the sample at roughly 200°C/s and switch the power off after 4 seconds. However, if the temperature ramp was maintained at 200°C/s for the whole heating period, the peak temperature would overshoot the aim by between 25 – 40 degrees. It was found that the extent of overheating varied considerably between the two materials, which made it impossible to compensate for the overshoot by adjusting the aim temperature downwards. In order to

vary the cooling rate between those obtained using forced air and by cooling in a vacuum, an appropriate cooling rate had to be preset in the heating profile.

This cooling rate was not obtained by varying the volume of the air flow but by adjusting the power supplied to the sample while the constant air flow was being maintained. This results in the linear cooling rates which can be seen in the cooling rate graph in Figure 16. Once the sample temperature had reached 400°C, the power was switched off and the cooling rate becomes the forced air cooling curve.

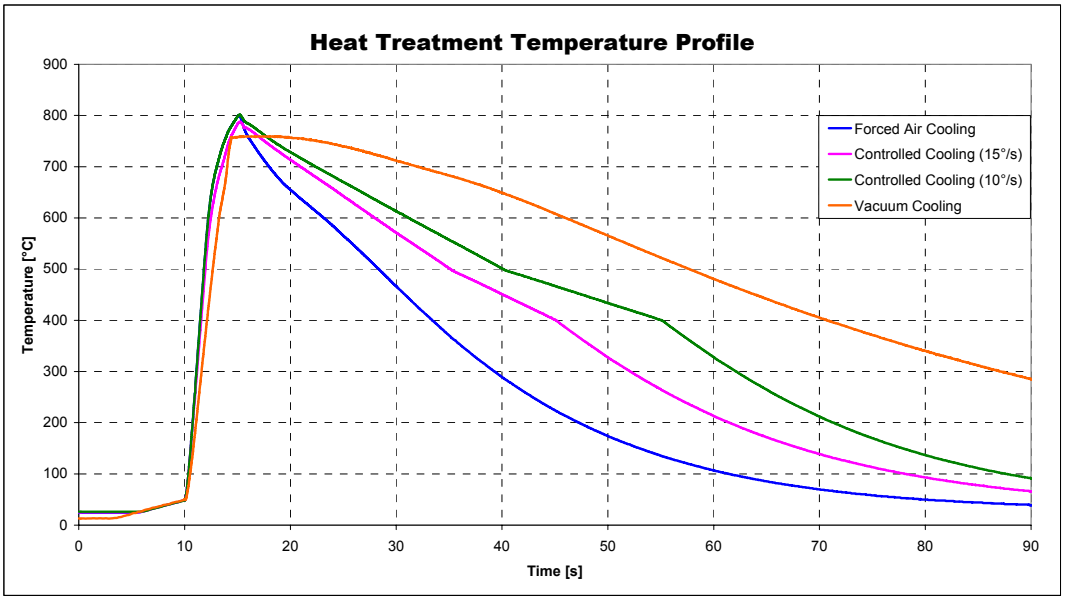

Figure 16 : Heat Treatment Temperature Profile For Various Cooling Rates

The differences between the cooling rates observed at the various thermocouple positions are illustrated in Figure 17. Given that the controlling thermocouple is at the centre of the sample, it would be expected that the peak temperature and the slowest cooling rate would be observed at this point. While the difference is not severe, it is

anomalous that thermocouple 1 shows a slower cooling rate than thermocouple 2. It is feasible that the position of air jets surrounding the sample was slightly off centre and therefore resulted on less efficient cooling at the position of thermocouple 1. In addition to this, the thermal resistance and the high heating rates applied could result in more rapid heating towards the edges of the sample. The curve for the vacuum cooled sample in Figure 16 shows that after the power was turned off, the sample temperature (at T2) actually increases marginally before it starts cooling.

Better thermal control would have been obtained by reducing the section of the sample but due to time constraints for the additional machining required, it was decided to use samples at the original thickness.

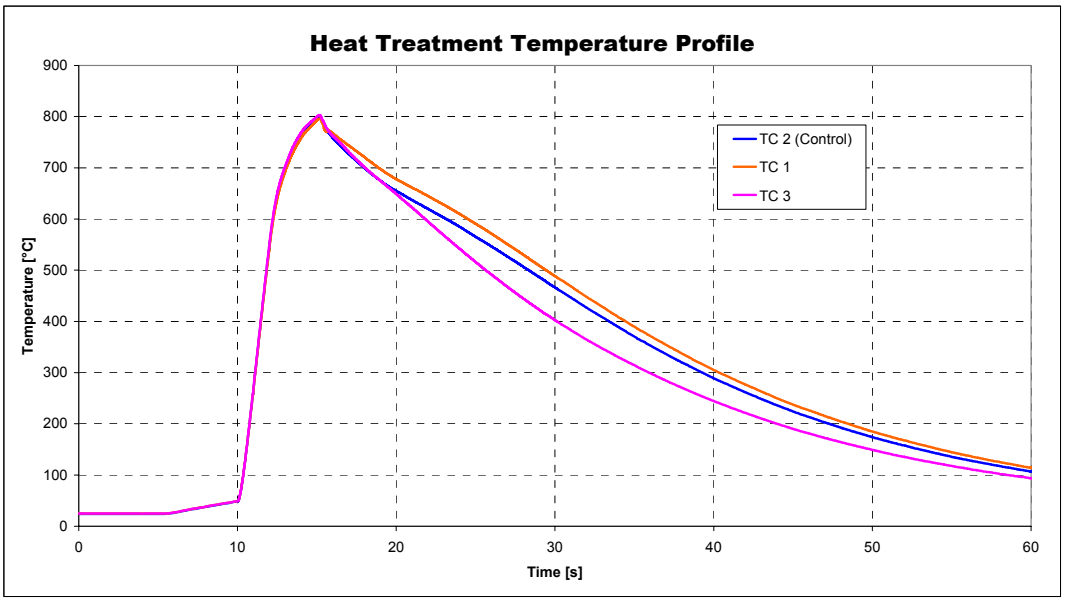

Figure 17 : Heat Treatment Temperature Variation By Thermocouple Position

The samples cut from the cross section were then mounted in cold setting resin and polished to 1μm finish. The edges of the exposed surface were marked off with lacquer to prevent crevice corrosion from occurring between the sample and the resin. A rectangular area of approximately 5x5mm was left exposed. A screw was mounted into the back of the sample before being set in resin and a wire was attached to the screw. All exposed metal on the screw and wire was coated in lacquer as well.

3.5 Electrochemical Testing

The Electrochemical Potentiodynamic Reactivation (EPR) evaluation technique has been successfully used on austenitic and dual phase stainless steels [51-53]. However, all these authors refer to the Double Loop (DL) EPR scan as opposed to the Single Loop (SL) EPR scan. Majidi and Streicher [51] evaluated the two methods on austenitic stainless steels and reported that the DL-EPR technique was superior to the SL-EPR method because it was more reproducible, less dependant on surface finish, unaffected by random pitting and independent of the grain size. In addition the SL-EPR technique required very close temperature control and restricted scan rates. Therefore, the DL-EPR technique was the only method used for all tests.

The samples were placed in a 50ml glass beaker surrounded by a platinum mesh. An $Ag/AgCl_2$ SCE reference electrode was placed close to the exposed material surface. The electrolyte was 0.1M H_2SO_4, 0.2M Na_2SO_4 with 100ppm KSCN and a pH of 1.6. The solution temperature was maintained at 25°C. The test solution was deaerated with nitrogen for 5 minutes before the scans were run. The potential was initially varied between -600mV and +900mV at a scan rate of 9V/hr (2.5mV/s) based on the recommended practice from literature [52] but then reduced to the range -600mV to +

600mV, after the initial results showed that no significant effects were taking place in the region above +600 mV.

Specimens were also cut from some samples of actual welds in such a way as to expose different parts of the weld to the reagent. These samples were mounted and polished as described for the Gleeble samples and included the unaffected base metal (for comparison) as well as sections of the weld toe at the root and on the upper side of the bead. The various sampling positions are illustrated in Figure 18 below.

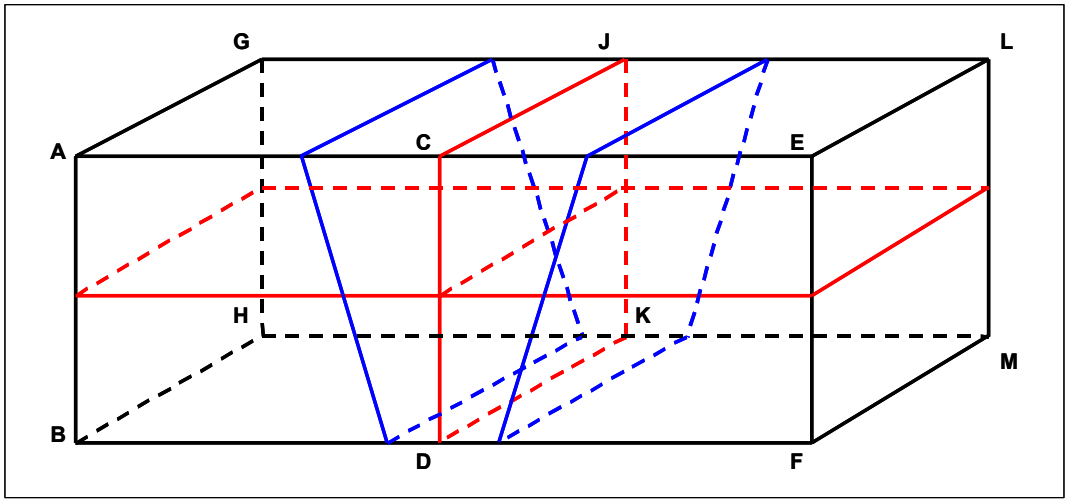

Figure 18 : Schematic Illustration Of Sample Positions With Reference To The Weld Bead

The sample was sectioned along the red lines and the samples then mounted so that the surface represented by e.g. ACJG was exposed during the test. The specific details for which surface was exposed during the particular test are given in Table 6 during the discussion of the results.

The extent of sensitisation is determined by the ratio of the reactivation current (Ir) and the activation current (Ia), where a low Ir/Ia ratio indicates a low degree of sensitisation. Since the ratio of the two currents is being used, the sample area and grain boundary dependence is circumvented.

4 Results and Discussion

4.1 Bead on Plate Welds

4.1.1 Welding Results

The multiple bead on plate welds were performed to provide some information regarding the interaction between the welds. Some literature [40] maintains that multiple welds should have a beneficial effect on the overall toughness of the weld by tempering existing martensite. A matrix of hardness tests was done in the area below the five weld beads and the positioning and results of the tests are shown in Figure 19 and Table 3 respectively. A similar matrix of tests was done on the sample where two additional beads had been laid down on top of the first set, but no significant differences could be seen between the results.

The microstructure shown in Figure 19 was revealed by etching with acidic ferric chloride, which clearly shows the coarse grained HAZ along the fusion line, but the distinction between the low temperature HAZ and the base metal was not clearly visible. The end of the LTHAZ could be determined by hardness measurements since the base metal had hardness in the range of 170HV while the martensite in the LTHAZ has a hardness of around 270HV. The hardness profile does however have some unusual anomalies where the hardness decreases between two points of high hardness with no obvious difference in the microstructure. It is to be expected that the hardness of the LTHAZ decreases with increasing distance from the fusion line as the volume of martensite formed decreases, but this was not always the case. Towards the centre of the sample, the hardness indentations fall on the CGHAZ which, being largely δ ferrite,

is significantly softer than the LTHAZ. This accounts for some of the low readings observed but doesn't explain the variation further away from the fusion line.

However, when the same samples were etched in 10% oxalic acid (electrolytic etch), a completely different pattern could be seen on the samples, as shown in Figure 20. The areas where fresh martensite had formed from the last weld beads to be deposited were essentially untouched by the etchant but areas which had been tempered and where carbide precipitation had occurred were strongly attacked. The areas showing up as dark grey in the macrograph were shiny and consist of fresh martensite, while the lighter matt grey areas are regions with extensive carbide attack.

While it may not be immediately obvious, the sample depicted in Figure 19 and Figure 20 is the same specimen with a different etch and with the edges truncated. The photographs have been stretched so that the hardness indents line up with the values in Table 3. It can be seen that the lower HV values fall predominantly in the light grey areas. The columns of 4 hardness indentations are spaced 1mm apart, which gives an indication of scale.

The areas where the HAZ from the various passes overlap are clearly defined, especially in the middle where the HAZ from the second and third passes have tempered the HAZ from the first weld, while a small untempered crescent from the first HAZ still remains. Since the extent of the LTHAZ is so clearly outlined, it becomes self evident from Figure 20 why no effect of the additional beads on top of the first set was detected. The layer of weld metal is significantly thicker than the HAZ and therefore the temperature in the parent metal would have been well below any

transformation temperature. The temperature could nevertheless have been in the sensitising region but no evidence of precipitation or sensitisation was seen which differed from the pattern observed in the original sample.

The data in Table 3 was plotted as a contour/area chart in an attempt to show the variation observed in the hardness readings. These results are shown in Figure 21. The correspondence between the results from the oxalic acid etch (Figure 20) and the area plot is difficult to observe since the interpolation between data points doesn't necessarily correspond with the actual situation. However, it can be seen that the light turquoise areas in the chart do correspond to the dark grey areas in the macrograph, which are the areas of untempered martensite.

The ASTM Standard A763 Practice W [43] describes an oxalic acid screening test for sensitisation which is designed to provide an immediate pass/fail test for sensitisation and as such it specifically targets precipitated carbides. However, ASTM A763 Practice W is too aggressive for low chromium steels and no conclusions can be drawn concerning sensitisation of the samples. As can be seen from the micrographs in Figure 22, the base metal and the tempered regions within the overlapping regions of the HAZ are equally attacked, with pitting on the grain boundaries and within the martensite grains.

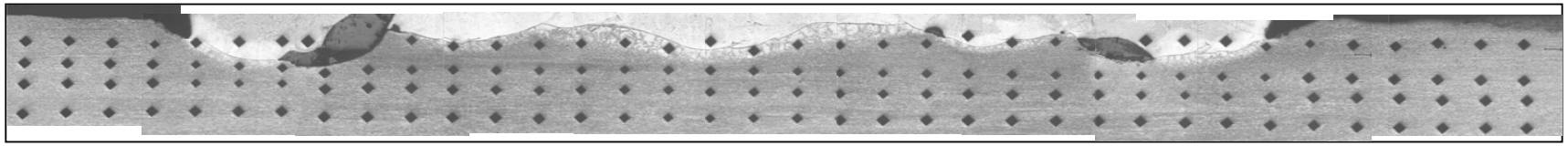

Figure 19 : Hardness Profile Across BOP Weld

174	175	172	256	208	187	177	166		230	208	209	223	237	221	189	193	193	223	260	229	222	195	203	241		180	191	192	243	272	174	180	171	172	171
166	168	169	178	264	234	242	204	188	234	227	218	233	272	260	217	200	215	264	267	269	227	226	233	251	259	275	272	269	275	179	174	176	176	169	176
178	172	181	170	258	271	272	176	170	176	195	207	228	232	222	229	231	222	222	230	241	204	192	175	183	241	263	263	263	187	176	180	177	177	180	174
178	179	180	183	178	172	173	178	174	174	173	173	178	218	260	267	240	209	184	171	169	174	173	168	170	172	170	172	174	181	183	186	181	180	181	181

Table 3 : Hardness Values (HV10) Corresponding To Indentations In Figure 19

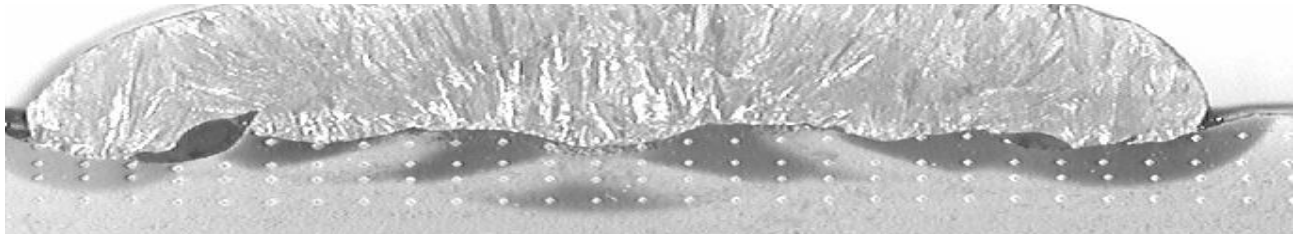

Figure 20 : BOP Weld, Etched In 10% Oxalic Acid (Electrolytic 15s) Dark Grey Areas Represent Fresh Martensite

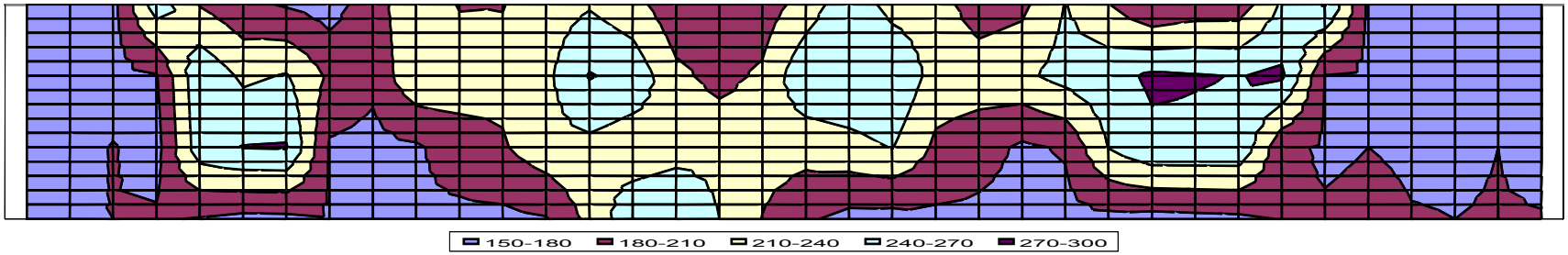

Figure 21 : Area Plot Illustrating Variation In Hardness Values On BOP Welds

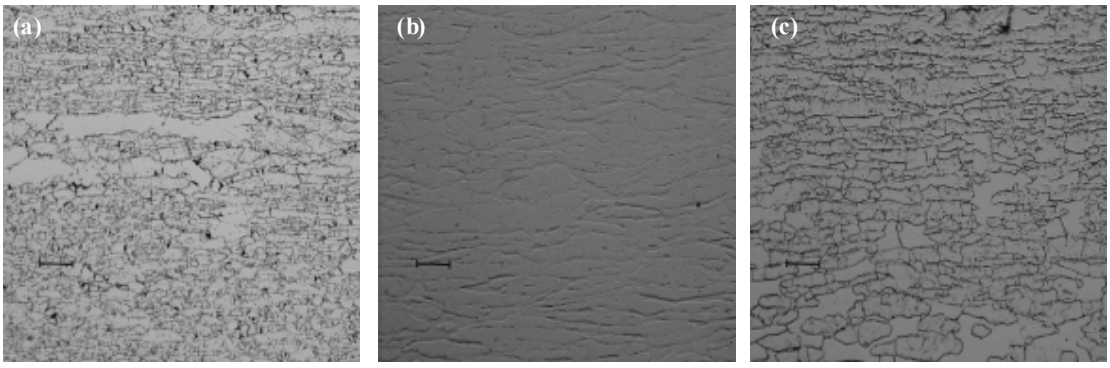

Figure 22 : Microstructure Revealed By Oxalic Acid Etch – (a) Base Material (b) Unattacked HAZ, Fresh Martensite With No Precipitates (c) Extensive Attack On Precipitates In Tempered Martensite (Distance Bar - 75μm, 100x)

After the samples had been examined by optical microscopy, all the samples were tested according to the modified Strauss test. A degree of mode 2 sensitisation in the overlapping weld HAZ regions was to be expected and copper deposition was seen on all the samples. After the samples had been cleaned and lightly polished, severe attack of the tempered HAZ regions was clearly visible. The corrosive attack didn't have the appearance of typical intergranular attack but appeared to be general attack on the martensite phase instead. The large δ-ferrite grains were largely unattacked but where ferrite-ferrite grain boundaries existed, these boundaries were clearly etched out. The regions where copper deposition occurred is shown in Figure 23(a) and the extent of the corrosive attack can be seen in Figure 23(b) after the copper deposit has been cleaned off. The samples were etched in acidified $FeCl_3$ for better contrast.

The copper deposition and corrosion pattern correspond with the regions of tempered martensite highlighted by the oxalic acid etch in Figure 20. The visible corrosion is clearly due to mode 2 sensitisation. No attack was seen on the HAZ from the beads laid

down at either end of the weld which indicates that mode 4 sensitisation was not occurring to a significant extent.

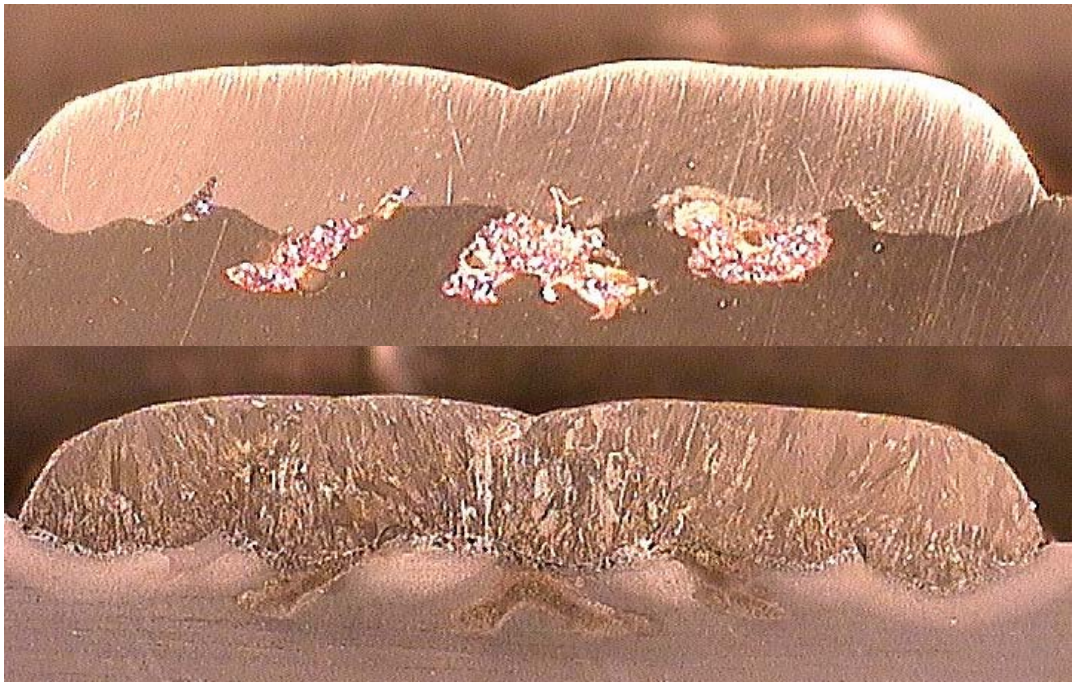

Figure 23 : (a) Cu Deposition At The Weld Intersections And (b) Extent Of Corrosion After Strauss Test

Since the weld metal deposit shown in Figure 23 is the result of five weld passes, it is surprising to note that there are only 3 obvious patches of copper on the surface of the sample. These areas correspond to the intersection of bead 1 with beads 2 and 3, respectively on either side. There is no obvious interaction and resultant sensitisation between beads 2 and 4, and 3 and 5. Figure 19 shows that there is a very large slag inclusion at the base of bead 5 on the left with a much smaller defect on the right. It may therefore be that the material temperature and hence the tempering characteristics are therefore strongly influenced by the presence of inclusions and defects.

4.1.2 Discussion: BOP Welding Results

The results in the section above concentrate almost exclusively on the sample which was welded at a heat input of roughly 1kJ/mm. Even though the other samples were tested in the same way, the results from the other samples did not provide any significantly different results. The weld quality on the welds done at lower heat input was particularly poor. The weld bead shape tended to be almost cylindrical, with a very sharp acute angle at the weld toe. Since the metal fluidity appeared to be fairly low, this sharp corner at the weld toe was either filled with flux inclusions or remained as an air gap (fusion defect) between the two beads. It can be seen in Figure 19 and Figure 20 how the slag inclusions at the weld toe influence the HAZ hardness and appear to act as an insulating layer. The scale of the defects was significantly worse than those shown in these figures and therefore these samples were not subjected to the same kind of scrutiny.

Even though it can be argued that this section of the work did not actually represent a realistic welding scenario, the results are useful in that they showed to what extent overlapping beads will interact and the extent to which tempering does occur in the HAZ from the previous weld bead. The subsequent Strauss testing confirmed where sensitisation could be expected, and even though this was the anticipated result, it was useful to have the theory confirmed. Another useful result was that no mode 4 sensitisation could be seen at the outer edges of the last beads to be deposited. Since mode 4 does occur as the result of a single pass, the high heat input used for the sample shown in Figure 20 could have resulted in mode 4 sensitisation at these points. As pointed out by Williams and Barbaro [27], the absence of copper deposition does not prove the absence of mode 4 sensitisation but even under microscopic examination no

intergranular attack was observed. However, since the material has a relatively high manganese and nickel contents, it will have a low Ac_1 temperature and therefore minimal sensitisation would be expected, in accordance with the proposed mechanism for mode 4 sensitisation.

There is no doubt that fairly extensive mode 2 sensitisation did take place in the overlapping areas of subsequent heat affected zones. However, in the apparent absence of mode 4 sensitisation, the sensitised regions do not reach the exposed surface and the weld bead would need to be completely removed before any intergranular corrosion could take place.

Full Butt Welds

4.1.3 Preliminary Welding Trials: Material A1

From the preliminary butt welding trials using flux cored wire, it was established that the root run gave the most problems with either inadequate fusion or material burn through. A good root run could be obtained when a dip transfer mode was set on the welding machine and subsequently, these parameters were used for the root run and the two subsequent cover passes on all the welds. The remainder of the passes were generally done using spray transfer mode settings.

The heat input and welding parameters are given in Table 4 below. From the literature [8] the arc efficiency for GMA welding is in the region of 60-75% and a factor of 75% was used in the calculation for heat input. The heat input value given in the table represents the average of all the passes excluding the root passes done using the dip transfer parameters.

The heat input was varied by adjusting the travel speed and the wire feed rate and the arc current and potential were determined by the welding machine. The values given in Table 4 for these two parameters are the final values displayed by the welding machine after welding had been completed.

Given that the recommended heat input range for 3CR12 type materials is 0.4 – 1.0 kJ/mm, these values are all on the lower side of the range. Nevertheless, the material deposition rate proved more than adequate to fill the V-notch, and at the higher heat input values, 8 passes were not required to complete the weld.

Table 4 : Welding Parameters Used For Preliminary Butt Welds

Sample ID	Heat Input	Current	Potential	Travel Speed	Wire Feed Rate
	kJ/mm	[A]	[V]	[mm/min]	[m/min]
BWA 01	0.63	110	25	200	6.1
BWA 02	0.48	107	25	250	6.0
BWA 03	0.55	104	25	220	6.2
BWA 04	0.40	114	20	250	6.5
BWA 05	0.37	112	22	300	6.5
BWA 06	0.61	109	25	200	6.5
BWA 07	0.68	117	26	200	7.2
BWA 08	0.39	105	24	300	6.0
BWA 09**	0.38	107	22	280	6.2
BWA 10	0.45	109	25	270	6.5
Constant Parameters for all Samples					
Gas Flow Rate : 15 l/min				Filler Material : 0.9mm 309L	
Contact Tip to Work Distance : 15mm				Interpass Temperature < 50°C	
** Dip Transfer Mode used for all passes					

Consistency in the weld bead positioning created the majority of the variation between the welds. In many cases the weld bead tended to ride up on one side of the V, leaving a very sharp notch at the base on the opposite side. Fusion defects were frequently noted at this position. The weld bead also frequently tended to wander and this created very uneven and lopsided welds, specifically with the last cover passes. This also created a situation where subsequent beads overlapped a great deal more than would be expected in an expertly welded joint. As was shown in the literature [33], the degree of overlap plays a significant role in whether sensitisation will occur. Examples of this will be shown in later sections.

Samples for metallographical examination were cut from each test piece which were then polished and etched in Oxalic acid. As with the BOP samples etched in this manner, the precipitate free untempered martensite was essentially unattacked. Unlike the BOP welds, a picture of how the HAZ from subsequent passes would interact in a

practical butt weld could be seen. It was not possible to predict the extent to which sensitisation had occurred, specifically in the transition between the base metal and the tempered HAZ regions.

However, in some cases it could clearly be seen where intersecting isotherms had reached the surface, which indicated sites where IGC would definitely be expected to occur. Two contrasting examples are shown in Figure 24. In picture (a), the HAZ is relatively small and the intersecting areas are substantially below the plate surface. In picture (b) it can be seen that the root run generated a very large HAZ while the HAZ from the back pass is significantly smaller. As a result, a narrow sensitised strip has been created on the bottom surface of the plate and this was confirmed by copper deposition on the underside of the sample during the Strauss test. The copper deposition patterns for the welds depicted in Figure 24 are shown in Figure 25.

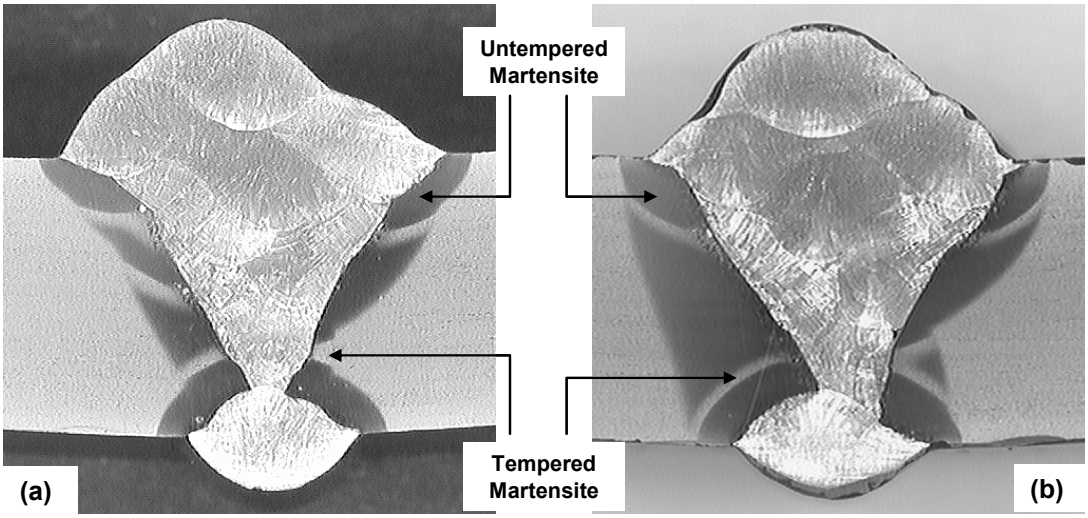

Figure 24 : HAZ Interaction Highlighted By Oxalic Acid Etch

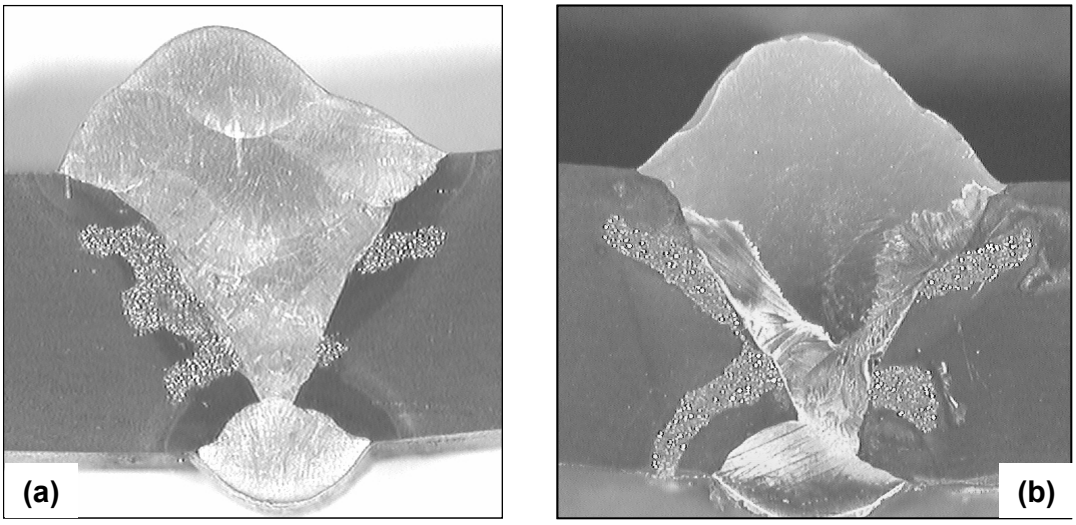

Figure 25 : Cu Deposition On Overlapping HAZ After Strauss Test

Three samples from each weld run were tested according to the modified Strauss test, as outlined in the previous chapter. Copper deposition could be seen on all the samples in the region of the root passes. A distinct difference could be seen in the degree of copper deposition on the samples where the weld cross-section was positioned vertically as compared to where it was horizontally positioned in the solution. The quantity of loose copper and other particles removed during cleaning was also greater and it is possible that these phenomena are linked. Despite the turbulence in the solution, any particles on the upper surface of the samples would have had a lower tendency to be removed than particles on a vertical surface. Since corrosion would already have been initiated in these regions, the covering copper deposits could have increased the corrosion rate by crevice corrosion effects which would in turn increase the copper deposition rate. The two samples shown in Figure 26 are for two samples cut from the same weld specimen and treated for the same time period in the same vessel. The sample on the left was

positioned horizontally while the sample on the right was vertical. The difference between the degree of copper deposition is clearly visible.

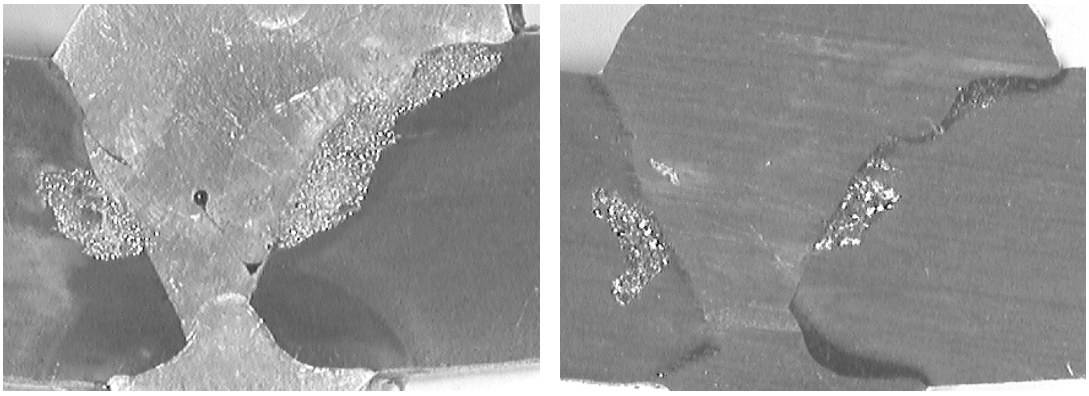

Figure 26 : Cross-Section Of HAZ Showing Less Cu Deposition On Vertically Positioned Sample

When the samples were examined under an optical microscope, it could clearly be seen that extensive corrosion of the martensite phase had occurred, as was the case with the BOP samples. In the most severe cases, the martensite regions were effectively completely corroded and only a network of δ ferrite grains remained. Theoretically, the absence of martensite grains could be due to grain dropping after the grain boundaries had been totally dissolved. However, given that the material is predominantly martensite with islands of ferrite and the fact that grain boundary precipitation and chromium depletion is much more likely to occur on δ-δ boundaries, grain dropping should involve the ferrite grains and not the martensite. In addition, samples cut perpendicular to the exposed surface showed dissolved martensite grains while the ferrite grains above them were still in place. This is clearly seen in Figure 27.

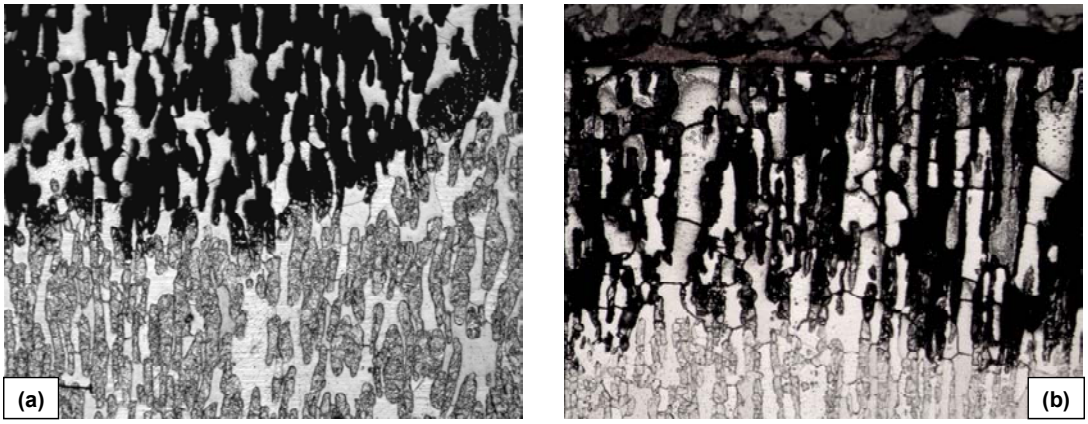

Figure 27 : Results Of Modified Strauss Test With Extensive Martensite Corrosion (a) Attack On Exposed Surface (b) Attack Perpendicular To Exposed Surface (200x)

The HTHAZ was similarly affected when the sensitising isotherms intersected through these regions. As can be seen in Figure 28, the martensite grains beading the coarse δ-ferrite grains along the fusion line are essentially removed. However, the ferrite grains also appear to be marginally affected by corrosive attack along what appear to be sub-grain boundaries.

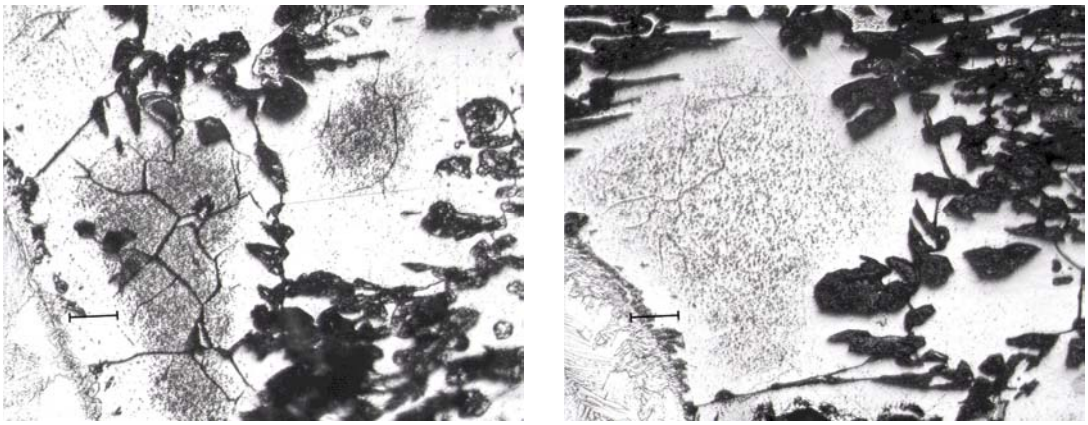

Figure 28 : Corrosion Of Martensite Surrounding δ-Ferrite In HTHAZ (Distance Bar – 38μm, 200x)

This level of corrosive attack could readily give rise to the conclusion that the material was not sensitised but rather that preferential corrosion of the martensite was occurring due to the reduced chromium content. However, if no element partitioning occurs during welding, as maintained by Gooch [40], the martensite on the whole sample should suffer similar corrosive attack, and not just specific regions within the HAZ. In areas where the martensite had been less severely corroded, it could be seen that the martensite phase was not being uniformly corroded but rather that corrosion was taking place on a network of sub-grain boundaries, as shown in Figure 29(a). In some instances a web of copper deposition could clearly be seen on the martensite grains as in Figure 29(b), indicating that corrosion was not uniform over the whole phase.

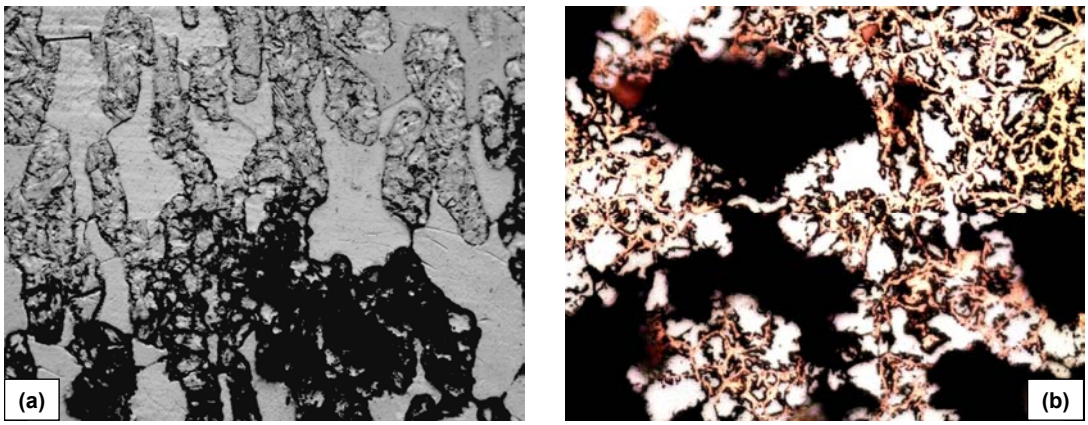

Figure 29 : (a) Preferential Corrosion On Martensite Phase Along Sub-Grains (Scale Bar – 20μm, 500x) (b) Cu Deposition Along Sub-Grains Within Martensite (1000x)

Samples were also examined under the SEM and typical results are shown in Figure 30. Extensive pitting of the martensite can be seen on the transverse section (Figure 30(a)) while the intergranular nature of the attack is clearly evident in picture (b), which was taken perpendicular to the weld cross section.

The extent of the copper deposition on the samples during the Strauss test (as shown in Figure 23 and Figure 25) indicates that reasonably large areas are sensitised. However, within these regions, the extent of corrosion could be extremely uneven with large crevices or irregular pits forming within regions of general attack. The SEM photographs in Figure 31 represent the section from the sample in Figure 24(b) on the bottom right hand side of the weld bead, just above the HAZ from the back pass. In Figure 31(a), extensive corrosion is visible in the bottom left hand corner while fairly severe but isolated crevices have formed at the extremity of the sensitised region.

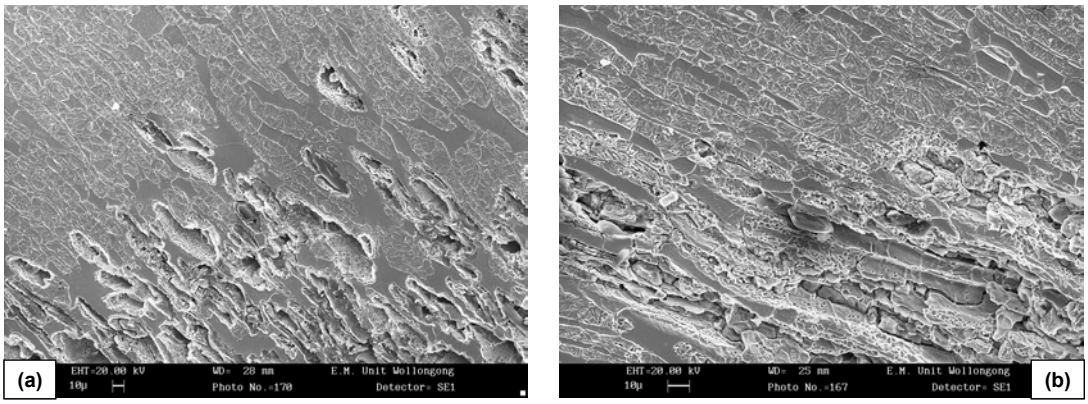

Figure 30 : Corrosion Attack On Martensite (a) Surface Directly Exposed During Strauss Test (b) Surface Perpendicular To Exposed Surface

The uneven nature of the martensite corrosion and the intergranular corrosion evident in Figure 30(b) indicate strongly that preferential corrosion of the martensite due to lower chromium content cannot be the only factor involved. In addition, if any element partitioning had taken place during cooling, the HAZ of all the weld beads should be affected, and not just the intersecting areas between beads.

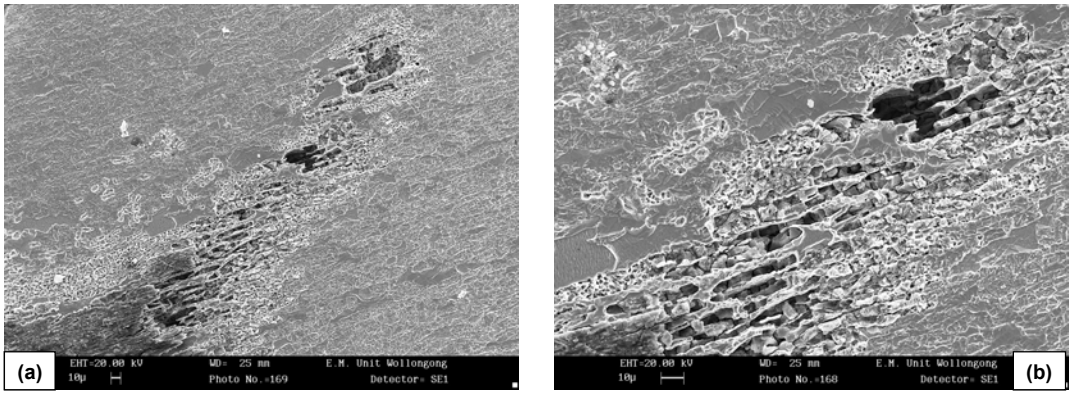

Figure 31 : Variation In Extent Of Corrosion Within Sensitised Regions

Any doubt as to whether corrosion was due to sensitisation could be settled by applying a healing heat treatment to the material. To confirm this, pieces were cut from several weld samples and annealed at 700°C for 10 minutes. The samples were then ground to remove the annealing scale and subjected to the Strauss test. As expected, none of the annealed samples showed any copper deposition and no IGC could be detected after polishing and examination under a microscope. Figure 32 shows that no IGC occurred in both the high and low temperature HAZ after the samples were annealed.

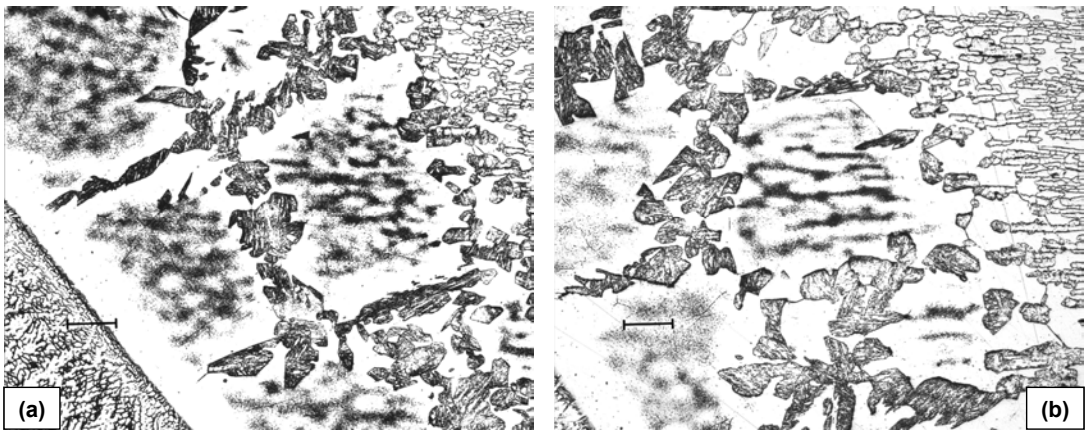

Figure 32 : CGHAZ After Annealing Free Of Corrosion (a) Scale Bar 75µm (b) Scale Bar 50µm

4.1.4 Comparative Welding Trials: Material A2 And C1

For the comparative work, the welding procedures used were the same as those outlined for the previous section i.e. pulse (dip transfer) mode was used for the root passes and spray transfer weld mode was used for the remaining passes. However, a ceramic backing strip was used on all the welds and hence better penetration was obtained on most welds. Superficial grinding was done on the root pass before the back pass was laid down.

However, the weld bead tended to wander and bead positioning was not good, which gave rise to a high level of inconsistency between the various runs. The aim was to produce similar welds in the two different materials from two manufacturers. The welding parameters used are given in Table 5 and comparable heat input values were obtained but the effect of these parameters is masked by inconsistencies in the welds.

As for the previous procedures, samples were cut from all the welds for metallographic analysis and Strauss testing. Samples from the two materials with comparable heat input in the welds were tested simultaneously. From purely visual observation of the samples when they were removed from the test solution, it was clearly visible that the samples from material C had significantly greater areas of copper deposition on them than material A. The samples as a whole also looked different, in that for material A, the polished surfaces were dull grey while on material C the samples were almost black.

Table 5 : Welding Parameters For Comparative Trials On Materials A2 And C1

Sample ID	Heat Input	Current	Potential	Travel Speed	Wire Feed Rate
	kJ/mm	[A]	[V]	[mm/min]	[m/min]
BWA 201	0.59	113	25	220	6.5
BWA 202	0.40	115	25	320	6.5
BWA 203	0.77	132	26	200	7.5
BWA 204	0.47	113	22	240	6.5
BWC 101	0.57	111	25	220	6.5
BWC 102	0.39	112	25	320	6.5
BWC 103	0.48	113	22	240	6.5
BWC 104	0.79	137	25	200	7.5
Constant Parameters for all Samples					
Gas Flow Rate : 15 l/min				Filler Material : 0.9mm 309L	
Contact Tip to Work Distance : 15mm				Interpass Temperature < 50°C	
Ceramic Backing Strip on Root Pass				Root Gap : 2mm	

From the analysis of the materials given in Table 1, it can be seen that material A contains significantly more chromium and slightly higher nickel which would have a significant effect on the overall corrosion resistance of material A. The difference in material discolouration is most likely due to this differing corrosion resistance. It is also likely that material C is inherently more susceptible to IGC since Demo [5] maintains that higher levels of carbon can be tolerated with higher chromium content, but material C has a higher carbon and nitrogen content as well as having less chromium. The difference in the level of copper deposition is illustrated in Figure 33. The samples shown are BWA 202 and BWC 102 which were welded with a heat input of roughly 0.4 kJ/mm.

Within the range of heat input used, very little difference can be detected between the level of copper deposition at lower heat inputs compared to higher heat input. What was far more evident was that bead positioning and the degree of overlap of the beads is extremely important in order to prevent mode 2 sensitisation on the surface of the

material. In this set of trials, several samples showed copper deposition on the upper or lower surface of the plate, parallel to the weld beads, but these defects could be attributed to poor welding rather than to an inherent material defect or the variation in the welding parameters.

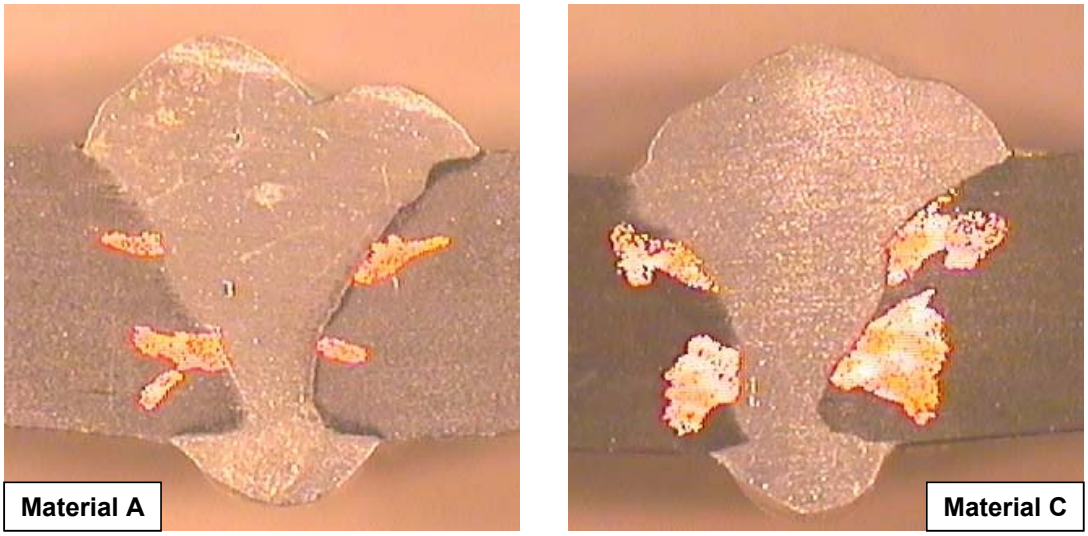

Figure 33 : Differences In Cu Deposition For Different Materials

As was discussed previously, it has been shown [33] that the extent of overlap is a significant contributing factor in causing sensitisation. This can be seen in Figure 34 where poor positioning of the final pass resulted in a high degree of overlap on the weld bead below and subsequently the sensitising isotherm intersected with the surface of the plate close to the toe of the weld. If the bead had been positioned correctly, the sensitising isotherm would have intersected with the lower weld bead and not reached the surface.

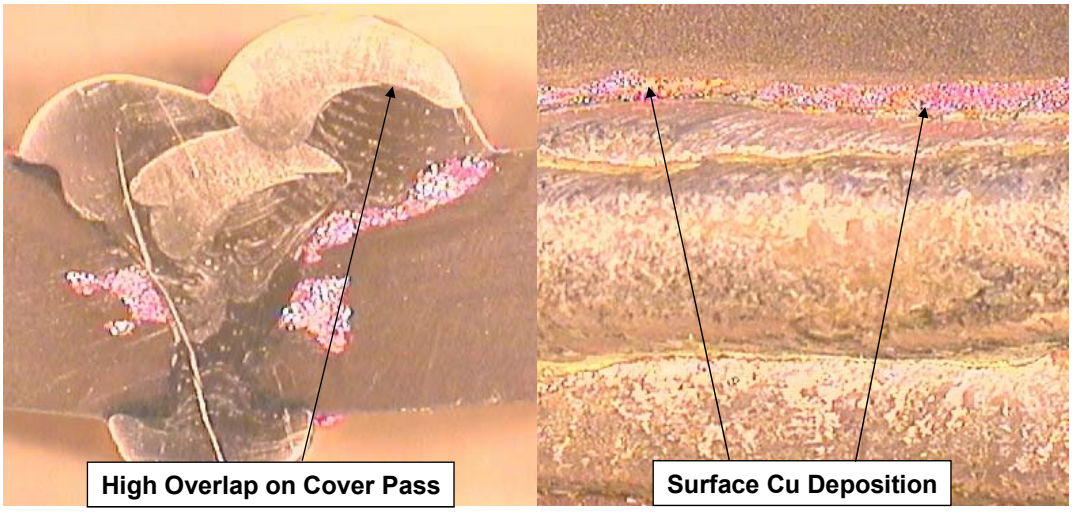

Figure 34 : Mode 2 Sensitisation At Weld Toe Due To Poor Positioning And High Degree Of Overlap.

The effect of bad positioning of the back pass is shown in Figure 35 below. The base of the root pass was not properly ground out and a serious fusion defect can be seen on the left of the root pass. The back pass position was badly off centre of the root pass and subsequently the HAZ from the back pass didn't engulf the HAZ from the root pass, as was the case in welds with reasonable positioning of the back pass.

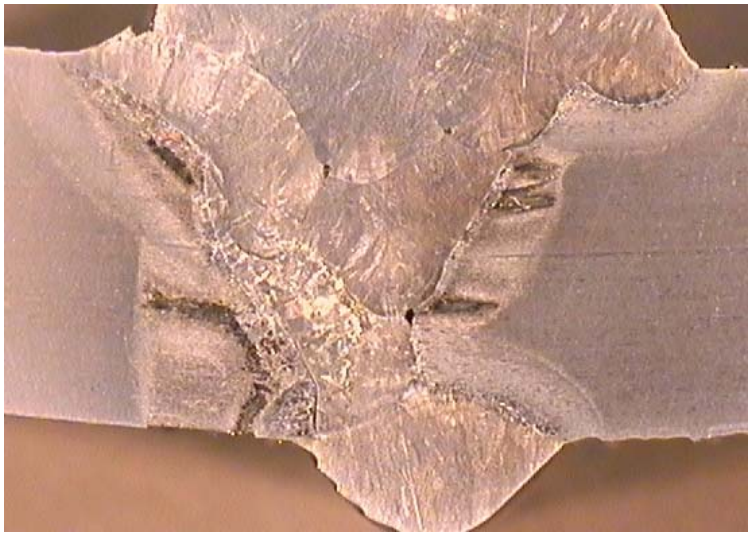

Figure 35 : Mode 2 Sensitisation Occurring As A Result Of Bad Weld Positioning

A very extensive sensitised region had been created off the toe of the back pass and severe corrosion was evident, as shown in Figure 36.

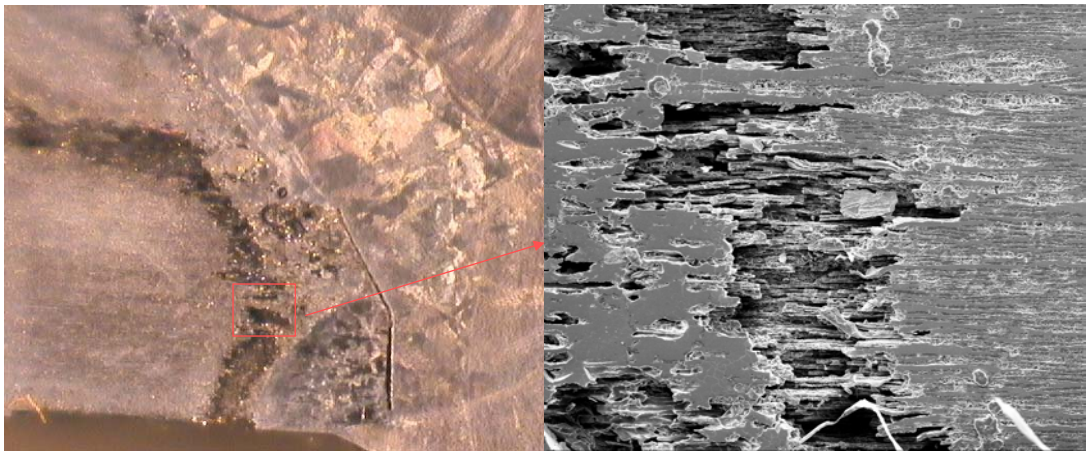

Figure 36 : Extensive Corrosion At Weld Toe Resulting From Mode 2 Sensitisation

4.1.5 Full Butt Welds: Discussion

Once again, as with the BOP welds, mode 2 sensitisation could not be avoided in the interior of the weld, irrespective of the welding conditions. Similarly, the inconsistencies in weld positioning and fusion defects resulted in too much variation in the overall weld to try and correlate the heat input with any degree of sensitisation.

The two most significant results from the work on both sets of samples were confirmation of the concept that high heat input is detrimental to the corrosion resistance and that poor welding, that is, excessive overlap or weaving, can result in severe sensitisation of the previous weld beads at the surface of the plate.

Quite apart from increasing the time that the material will spend in the sensitising temperature range, unnecessarily high heat input will also result in a very large HAZ. While not necessarily detrimental on its own, a large HAZ with obviously very susceptible martensite increases the potential for sensitisation from subsequent parallel or intersecting weld beads. This problem has been clearly illustrated in Figure 25. The problems associated with excessive overlap and bad positioning have also been illustrated in Figure 34 and Figure 35.

As noted previously, despite the relatively low heat input parameters selected, in many instances the volume of metal deposited appeared to be excessive for the recommended number of passes. However, any attempt at reducing the metal deposition rate by increasing the travel speed or reducing the wire feed rate resulted in poor fusion and very bad welds. A competent welder would be in a position to overcome these problems and produce consistent welds with smaller, more regularly positioned beads which should produce significantly smaller HAZs and subsequently less sensitisation. As a result, the only sensitised regions within a professionally completed weld would be well below the surface. While this may not represent an ideal situation, the use of unstabilised material could still represent a cost effective solution over the additional problems associated with producing stabilised thick gauge plate.

One very significant difference that could be seen between the BOP samples and the butt welds was that some of the butt weld samples showed indications of mode 4 sensitisation. This was not the case on all the samples but could be seen on certain samples from both materials. One example is shown in Figure 37 below.

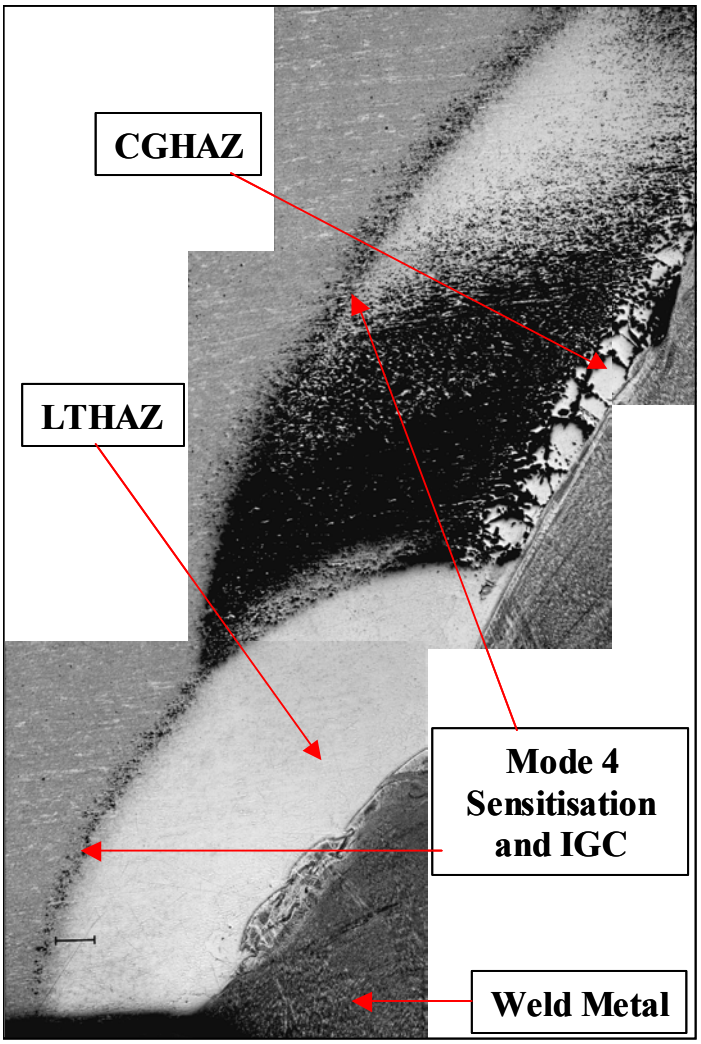

Figure 37 : Mode 4 Sensitisation At The Surface Of Sample BWA 09

As with the mode 2 sensitisation, the mode 4 attack does not show typical intergranular corrosion but manifests as general dissolution of the martensite grains. In this instance it can be seen as a fine row of pits along the edge of the LTHAZ. What is particularly unusual about the presence of mode 4 in this instance is that this sample was welded at a significantly lower heat input than the BOP material shown in Figure 23 and that sample did not show a similar effect. High heat input, together with a high Ac_1 temperature are the factors which are believed to influence the creation of mode 4 and neither of these

should be a factor on sample BWA 09. However, the one significant difference between this sample and all the other samples from the same batch is that a dip transfer mode was used for all the passes, and not just for the root passes but it is not clear whether this could have resulted in the observed IGC.

A similar example which occurred on material C is shown in Figure 38 below. This effect could be seen on practically all the samples from material C, irrespective of the welding parameters but the level of pitting attack didn't appear as severe as on sample BWA 09. The region of mode 2 sensitisation highlighted in Figure 38 occurs much closer to the surface than could be considered acceptable but this HAZ has been sensitised by the subsequent weld bead which was deposited almost directly above it. This once again shows how the weld bead positioning can lead to sensitisation.

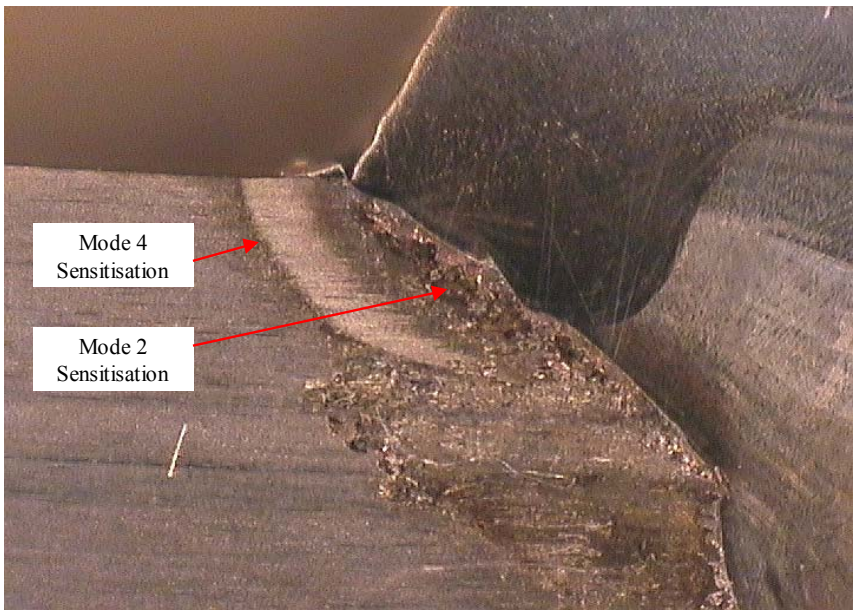

Figure 38 : Mode 4 Sensitisation And IGC On Material C

4.2 Electrochemical Evaluation

4.2.1 Electrochemical Potentiodynamic Reactivation (EPR)

4.2.1.1 Butt Welded Samples

The current density results for the welded samples are given in Table 6 below. The sample positions refer to the coordinates that are illustrated in the previous section in Figure 18. As shown, sample A202 included the complete weld and HAZ on both sides of the root run, unlike the other samples where the weld was sectioned down the middle. Sample A109 # 1 was taken from the base metal more than 30mm from the edge of the weld bead and was included for comparison, representing material which would not be expected to have any sensitisation.

Due to time constraints, only a limited number of samples were selected for EPR analysis. The overall weld quality was an important criterion for selecting samples for EPR testing in order to exclude any welds where definite mode 2 sensitisation had been observed at the surface of the sample. It was not considered important to do a large number because the Gleeble samples were expected to deliver more repeatable and representative results. Even though the double loop EPR method is supposed to be independent of parameters like grain size and sample area [51], better results were expected from samples with a larger sensitised region.

Table 6 : EPR Test Results For Welded Samples

Sample	Number	Heat Input [kJ/mm]	Sample * Position	Area [mm^2]	Ir / Ia			Average
A 109	1	0.4	Base Metal	33.77	0.3816	0.2921	0.2088	0.2942
A 109	2	0.4	BDKH	37.40	0.0839	0.0635	0.0602	0.0692
A 109	3	0.4	DFMK	66.61	0.0446	0.0447	0.0565	0.0486
A 109	4	0.4	ACJG	40.81	0.0368	0.0429	0.0495	0.0431
C 101	1	0.6	DFMK	47.24	0.4435	0.5728	0.6005	0.5389
C 101	2	0.6	BDKH	48.50	0.2656	0.3468	0.3954	0.3359
C 101	3	0.6	CELJ	48.46	0.1314	0.1602	0.1814	0.1577
A 202	1	0.4	BFMH	95.68	0.0178	0.0152	0.0151	0.0160
C 104	1	0.8	DFMK	53.89	0.2638	0.2370	0.1687	0.2232
C 104	2	0.8	CELJ	43.40	0.1689	0.0654	0.0447	0.0930

*** Sample Position refers to the area coordinates shown in Figure 18**

From the literature [52] the EPR scan curves were expected to resemble the curves as shown in Figure 39. The curves plotted in the figure below are for the three scans done on the same sample and the activation and subsequent reactivation curve have been plotted in different colours so that any overlap is readily distinguishable. In many cases the scan signal showed a great deal of noise, with the measured current density fluctuating wildly. This can occur as a result of gas generation on the surface of the sample and bubbles between the sample surface and the SCE affect the current flow in the system. The noise tended to be worst in the potential range between 0 and +0.5V and therefore the activation and reactivation potential could still be determined. In some instances no reliable value could be determined and the sample results were neglected.

The graphs show a fairly clear shoulder in the reactivation curve, which has been indicated by the grey shaded area on the left hand side of the curve in Figure 39. According to Frangini et al [52] this shoulder is due to preferential corrosion and

reactivation of the martensite, which is occurring before the reactivation potential on the grain boundaries is reached.

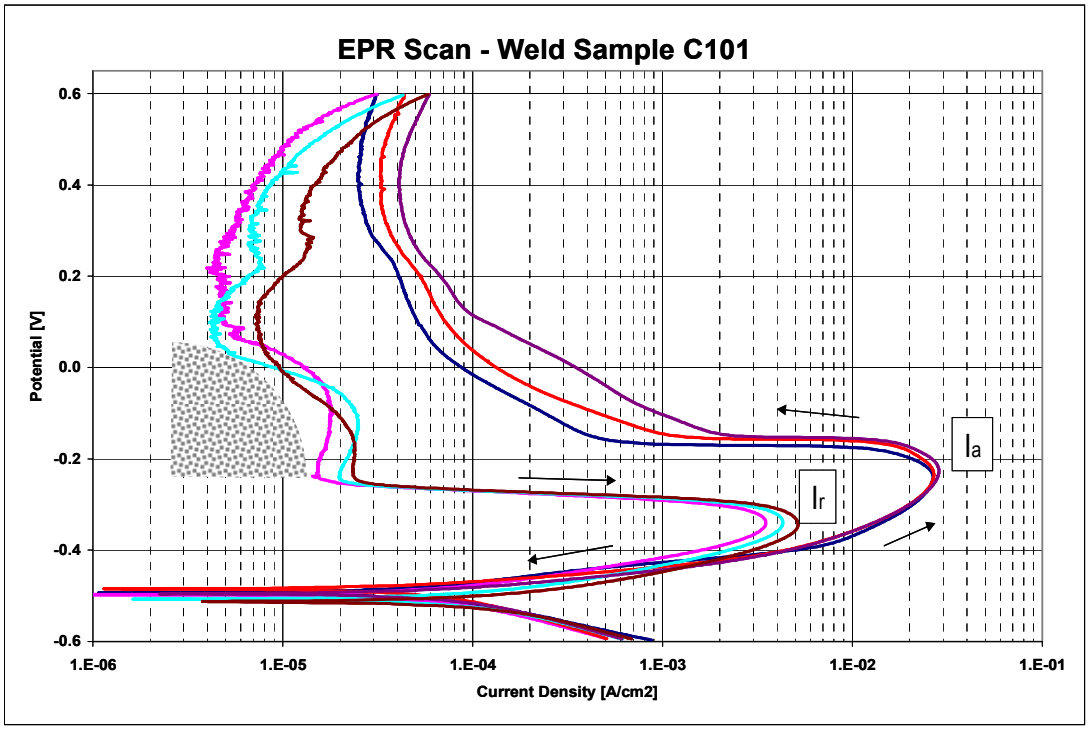

Figure 39 : Typical EPR Scan Chart

In addition to the shoulder visible in Figure 39, some scans showed a clear cathodic loop as seen in Figure 40 below, and on some scans, even more than one was visible. The reason for why these cathodic loops only appeared intermittently is not clear. However, on the material illustrated below, the sample was prepared in such a way as to include the full root pass bead and approximately 3-4mm of the HAZ and base plate on either side (as shown in Figure 41). The material which is then exposed to the test contains material with vastly differing corrosion resistance, with the sensitised region of the HAZ being relatively low and the high chromium, high nickel austenitic filler

having good corrosion resistance. This mixture of material could well influence the recorded current density and create the effects illustrated in the figure below.

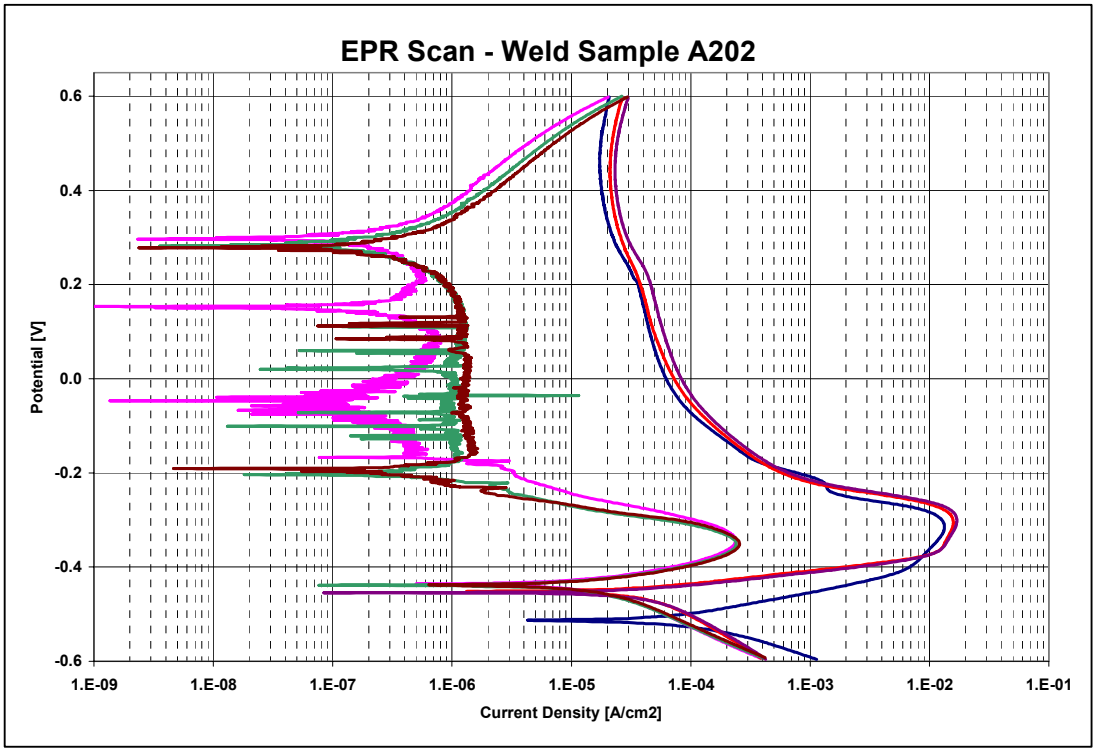

Figure 40 : EPR Scan For Material A202 Showing Strong Cathodic Loop

Apart from the quantitative results from the EPR scans, the EPR samples provided metallographical evidence that mode 4 sensitisation was present, even if only to a marginal degree. Figure 41 below shows a macro photograph of the root pass of sample A202 after the EPR scan shown in Figure 40 was done. The CGHAZ on either side of the weld, the extent of the LTHAZ and the sub Ac_1 region where mode 4 is expected to occur can clearly be seen.

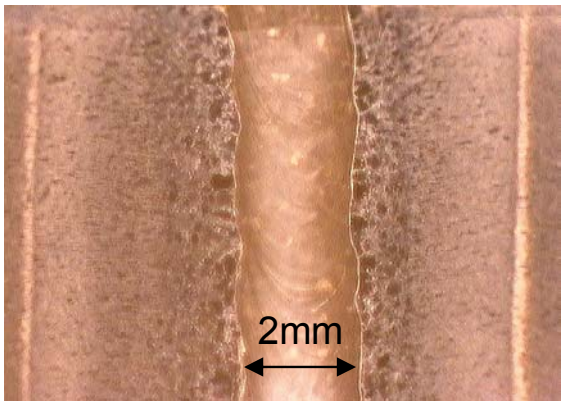

Figure 41 : Sample A202 After EPR Testing Showing Corrosion At The Edge Of The LTHAZ.

Even though the corrosion line is clearly visible to the naked eye, the actual extent of attack is very superficial. Transverse sections were cut from the sample shown above to examine the extent of the corrosion and to determine if obvious intergranular attack was occurring along the edge of the LTHAZ. However, no intergranular attack could be found penetrating into the material and the depth of the surface corrosion was so slight that it could not be reliably distinguished from the general corrosion irregularities of the LTHAZ and parent plate.

As was seen on the micrographs from the Strauss tests, the appearance of the corroded region resembled general corrosion of the martensite rather than very localised attack on the grain boundaries. This is illustrated in Figure 42 and Figure 43 below.

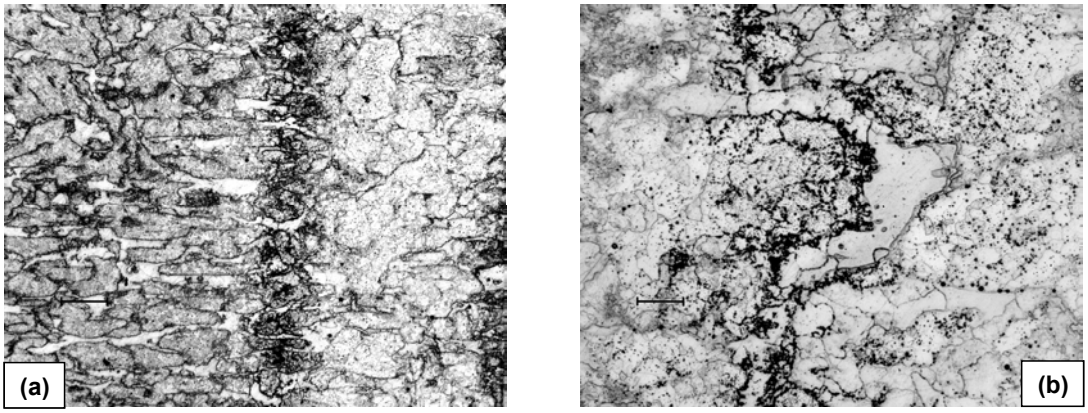

Figure 42 : Corrosion Attack On Sample A202 (a) 50x, Scale Bar 150μm (b) 200x, Scale Bar 38μm

While the corrosion line appears as a fairly well defined and corroded zone at low magnification as in Figure 42(a) above, at higher magnification i.e. Figure 42(b) it becomes apparent that the corrosive attack consists of a fine dispersion of pits within the martensite and on the martensite and ferrite grain boundaries. Figure 43(a) shows clearly how some ferrite subgrain boundaries are being fairly severely attacked in the narrow band of the sub Ac_1 temperature region while the extremities of the same grains which lie outside the zone are relatively untouched. At the high magnification in Figure 43(b) it can be seen that fairly widespread pitting of the martensite grains is occurring but intergranular attack predominates.

A similar pattern was also observed on sample A109 where a sample containing one half of the HAZ of the root pass was prepared. In this instance, the line indicating the corrosion attack appeared darker as seen in Figure 44(a) below (as compared with Figure 42(a)) and at higher magnification, more extensive pitting is evident. The appearance of the pits is however unusual in that they are very angular as if large cubic inclusions have been removed from the matrix. The very clear distinction between the essentially precipitate free ferrite (with clearly defined and etched grain boundaries) and

the martensite as seen in previous micrographs is not visible on this sample. No obvious reason for the angular appearance of the pitting can be found.

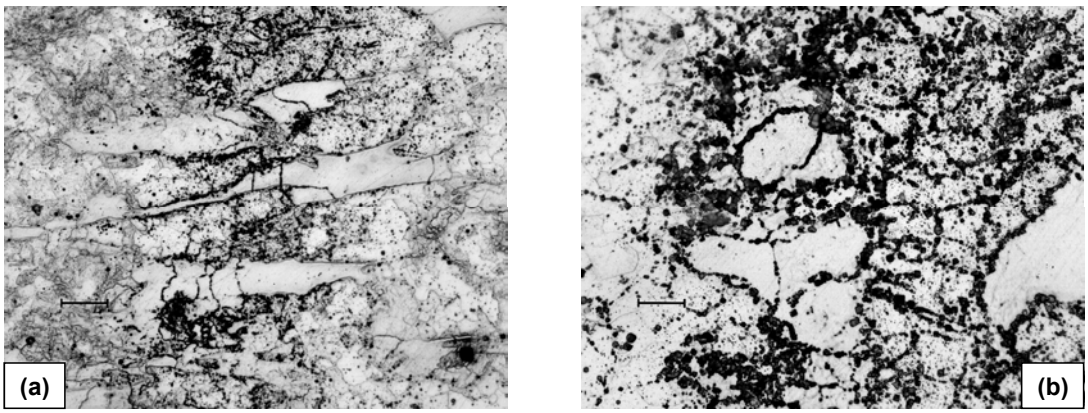

Figure 43 : Grain Boundary Attack On Sample A202 (a) 200x, Scale Bar 38μm (b) 500x, Scale Bar 15μm

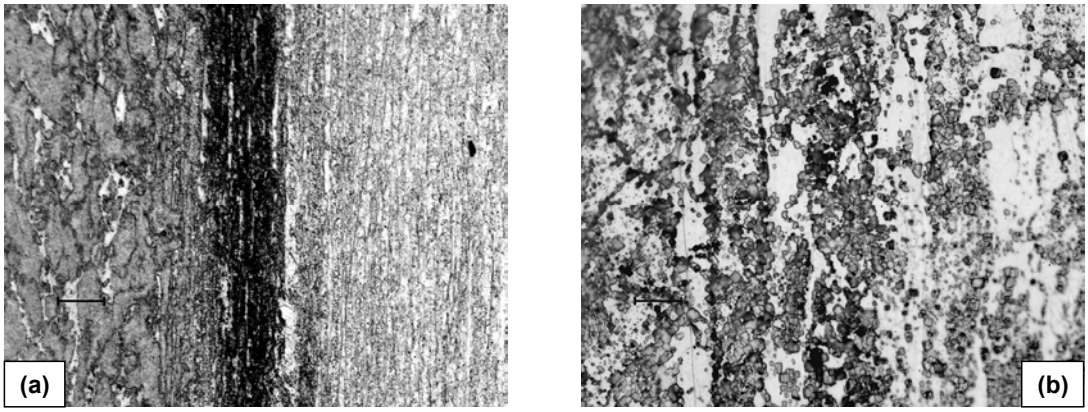

Figure 44 : Grain Boundary Attack On Sample A109 (a) 200x Scale Bar 38μm (b) 500x, Scale Bar 15μm

Figure 41 shows how the CGHAZ can be distinguished fairly clearly, even under very low magnification. However, the grain boundary definition was little more than would have been expected by a normal laboratory etch. By comparison, material C showed fairly pronounced attack of the δ ferrite grain boundaries, as shown in Figure 45 below.

It is feasible that this observed attack is due to mode 3 type sensitisation i.e. very rapid cooling of the HAZ but given the volume of martensite present in the CGHAZ, this should not be significant.

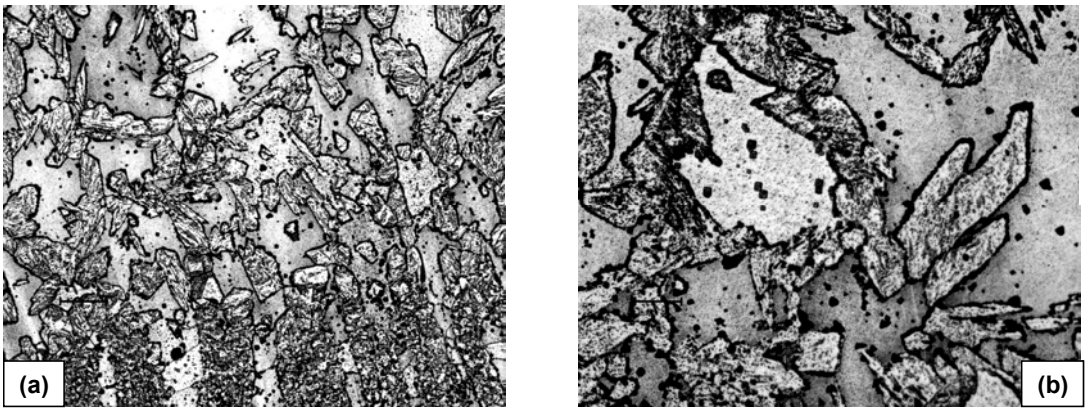

Figure 45 : Grain Boundary Attack In CGHAZ On Material C101 (a) 200x Mag (b) 500x Mag

4.2.1.2 Gleeble Simulation Samples

The EPR tests on the simulated weld samples suffered from similar problems as those experienced with the welded samples. Excessive noise and variation between repeated tests on the same samples has resulted in extensive scatter in the results. Results reported in the literature [51-53] show that the experimental set-up, specifically the KSCN concentration among other variables, can affect the test results. In order to obtain results which clearly indicate the degree of sensitisation, a series of EPR scans using varying KSCN concentrations would definitely be beneficial but insufficient time was available to include such a large number of experiments.

According to the theory for mode 4 sensitisation [27], slower cooling rates (resulting from higher heat input levels) will result in a higher degree of sensitisation. While the

results are theoretically very easy to plot and determine whether any correlation exists between cooling rate and the Ir/Ia current density readings, the results are complicated by variation in the maximum temperature obtained during the simulation. In addition, the results obtained on the parent metal and on the quenched sample cannot be included in any correlation. At best the values can be plotted by sample for illustrative purposes only. A summary of the results obtained for each material is given in the tables below.

Table 7 : Summary Of EPR Scan Results For Material A

Sample ID	Peak T [°C]	Time (8-5) [s]	CR (8-5) [°C/s]	Ir / Ia
BWA As Quenched				0.0019
BWA Base Metal				0.0140
BWA 032	756	38.3	6.7	0.4620
BWA 033	777	26.7	10.4	0.5165
BWA 062	826	13.4	24.3	0.0403
BWA 063	829	12.4	26.4	0.1136
BWA 092	801	13.7	22.0	0.1159
BWA 093	796	10.2	28.9	0.3280
BWA 111	788	19.0	15.2	0.1951
BWA 113	792	13.5	21.7	0.0378
BWA 122	801	24.9	12.1	0.2028
BWA 123	791	16.3	17.8	0.0956

The values given for cooling time and cooling rate have been determined as the time taken for the sample to cool from the maximum temperature (with the aim temperature being 790°C) to a temperature of 500°C and the cooling rate (CR 8-5) is subsequently the average cooling rate achieved over the actual temperature range.

While a large degree of variation can be seen in the EPR results and the actual results do not correlate sufficiently to determine or predict the degree of sensitisation present in any particular sample, a reasonable trend can be seen between the cooling rate and the

current density ratio. As expected, the degree of sensitisation on the fully annealed and as quenched samples is significantly lower than on the other heat treated samples.

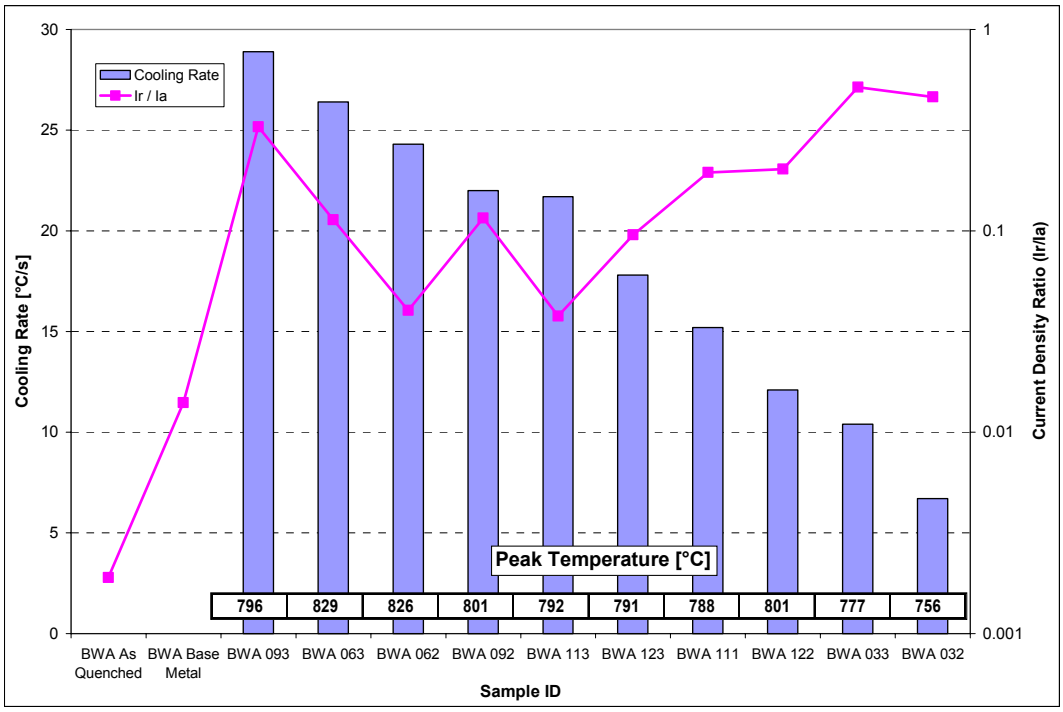

Figure 46 : Cooling Rate And Current Density Ratio For Material A

While largely in keeping with the theory of mode 4 sensitisation, it is perhaps surprising that the samples which only reached temperatures of around 760°C have such high EPR results, despite the very slow cooling rates. This temperature is of the order of an industrial annealing process and the cooling rates after annealing would be within the range used in these experiments, since forced air cooling is standard practice. It would therefore not be surprising if these samples showed similar EPR results to the parent plate, since there is no reason why any dissolution and precipitation of carbides should occur during welding and not during annealing, when the material is heated to a similar temperature and cooled at a similar rate.

Table 8 : Summary Of EPR Scan Results For Material C

Sample ID	Peak T [°C]	Time (8-5) [s]	CR (8-5) [°C/s]	Ir / Ia
BWC As Quenched				0.0620
BWC Base Metal				0.0736
BWC 032	759	42.2	6.1	0.4846
BWC 033	756	38.5	6.7	0.5295
BWC 061	826	14.3	22.8	0.4191
BWC 063	826	9.1	35.9	0.3569
BWC 092	787	14.0	20.5	0.2421
BWC 093	781	8.7	32.3	0.1644
BWC 112	788	19.9	14.5	0.4669
BWC 113	785	14.3	19.9	0.3182
BWC 122	802	24.9	12.2	0.3996
BWC 123	795	17.6	16.7	0.4111

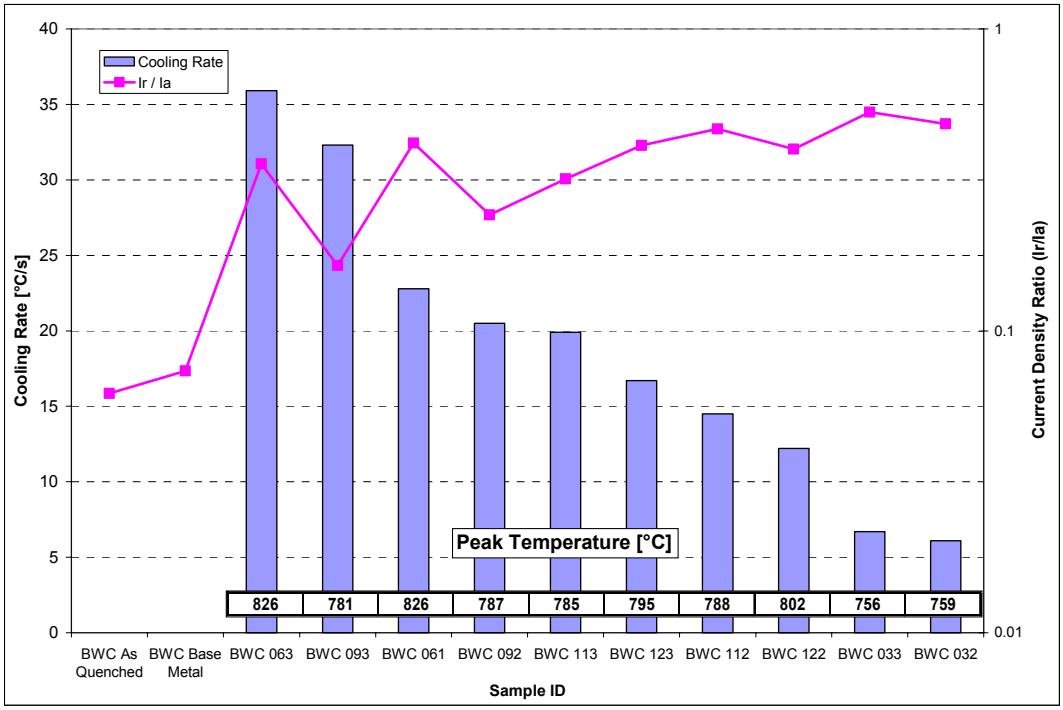

Figure 47 : Cooling Rate And Current Density Ratio For Material C

Despite the variation in the data values, overall the EPR results for material C are higher than for material A, specifically for the as quenched and parent plate. While this is possibly attributable to the overall lower alloying (specifically chromium and nickel) content in material C, theoretically this should not be occurring. The lower corrosion

resistance attributable to the lower alloying content should manifest as the shoulder in the reactivation curve as illustrated in Figure 39 and not as an increased Ir/Ia ratio. The difference in the EPR results would therefore appear to indicate that the degree of sensitisation in material A is lower than for material C.

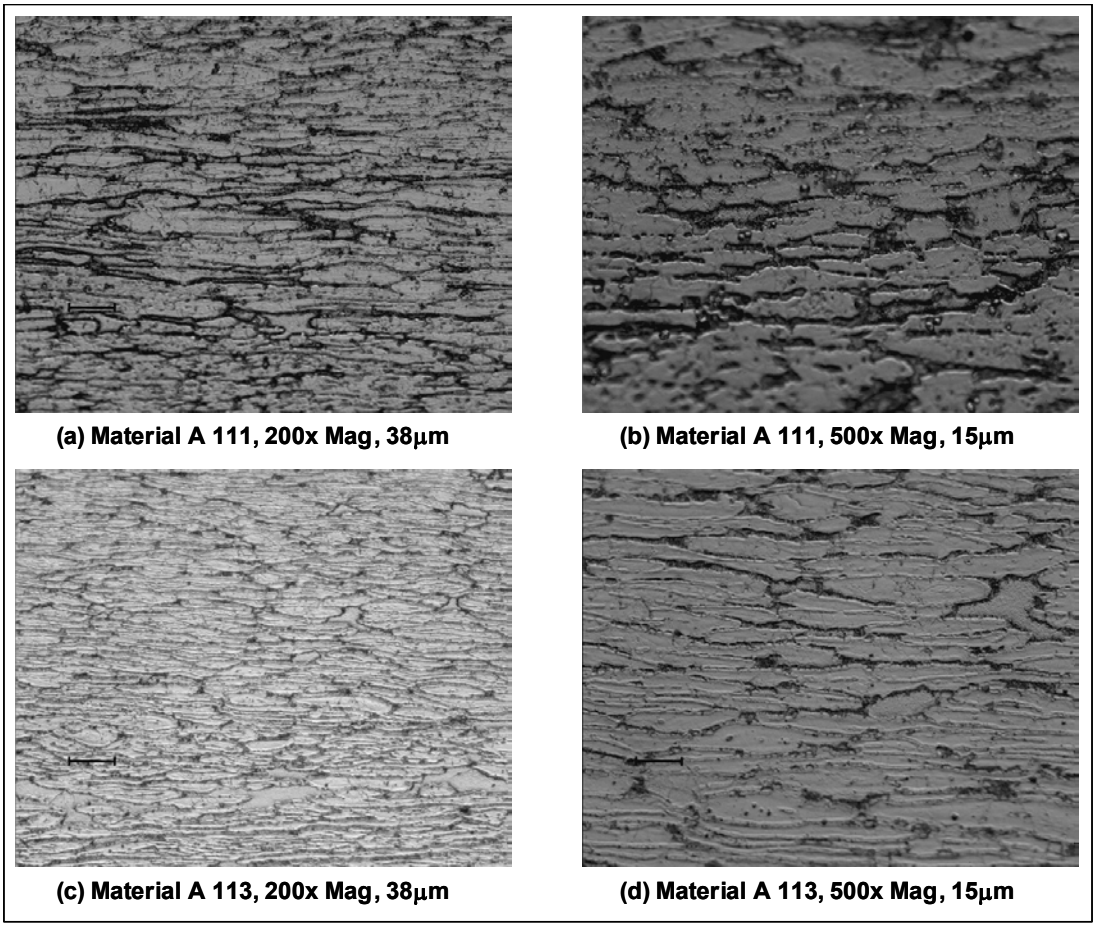

Figure 48 : Microstructures Of EPR Samples From Material A 111 And 113

When evaluating sensitised materials metallographically, the standard classifications [42, 43] for severity are

Step structure – steps between grains, no sensitisation

Dual structure – ditches at grain boundaries, but no grains completely encircled

Ditch structure – one or more grains completely surrounded by ditches

Majidi & Streicher [51] maintain that the ASTM weight loss measurement techniques for evaluation can distinguish between ditch and dual severity but isn't sufficiently sensitive for step severity rating. Conversely, EPR methods become ineffective at high levels of sensitisation, i.e. the distinction between dual and ditch classification is blurred. However, when the EPR samples were evaluated after the scans had been completed, the observed microstructures were difficult to classify according to these standard classifications.

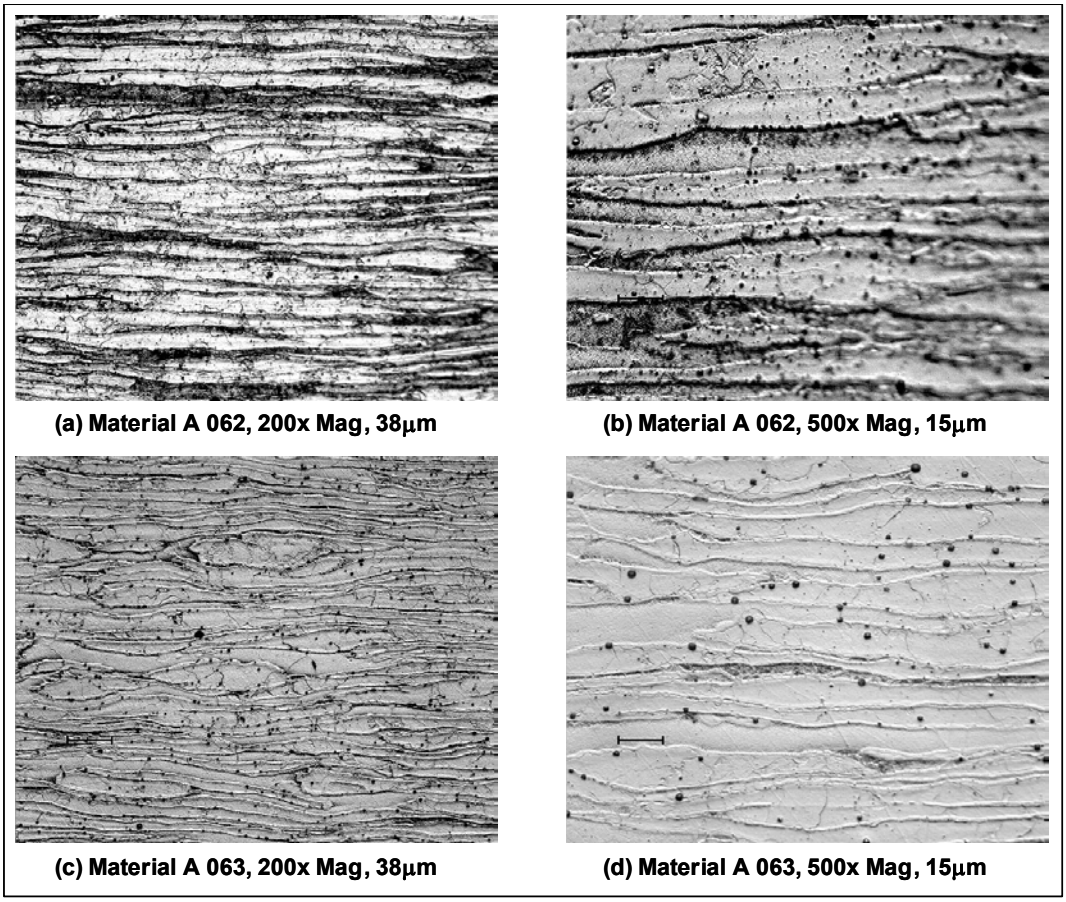

Figure 49 : Microstructures Of EPR Samples For Material A 062 And 063

As was observed for the Strauss test samples, fairly extensive general corrosion was visible on the martensite phase and as such evaluation of the extent of grain boundary attack was less straightforward. An example is shown in Figure 48. The Ir/Ia value for material 111 (a and b) is 0.1951 while for sample 113 (c,d) the value was 0.0378. and difference in the degree of grain boundary attack is obvious. Sample A111 would have to be classified as having a ditch structure while A113 could still be considered as dual.

The micrographs in Figure 49 for material A062 and 063 show a similar picture with 063 again having an Ir/Ia value significantly lower than that for A062. However A062 appears to have a greater degree of general corrosion of the martensite than material A111, and as such the extent of pure grain boundary attack is less obvious.

It is also not clear why there is such a difference between the Ir/Ia values for A062 and A063 (and obvious difference in the degree of grain boundary attack) since the cooling rates are fairly similar. While Figure 49(c) appears to show a relatively high level of grain boundary attack, in Figure 49(d) it appears that the attack is occurring as general corrosion on very elongated grains of martensite.

Given that sample A06 reached a peak temperature approaching 830°C at both positions where the samples A062 and A063 were taken, it is possible that the Ac_1 was exceeded and that some austenite transformation occurred and the resulting martensite is being attacked.

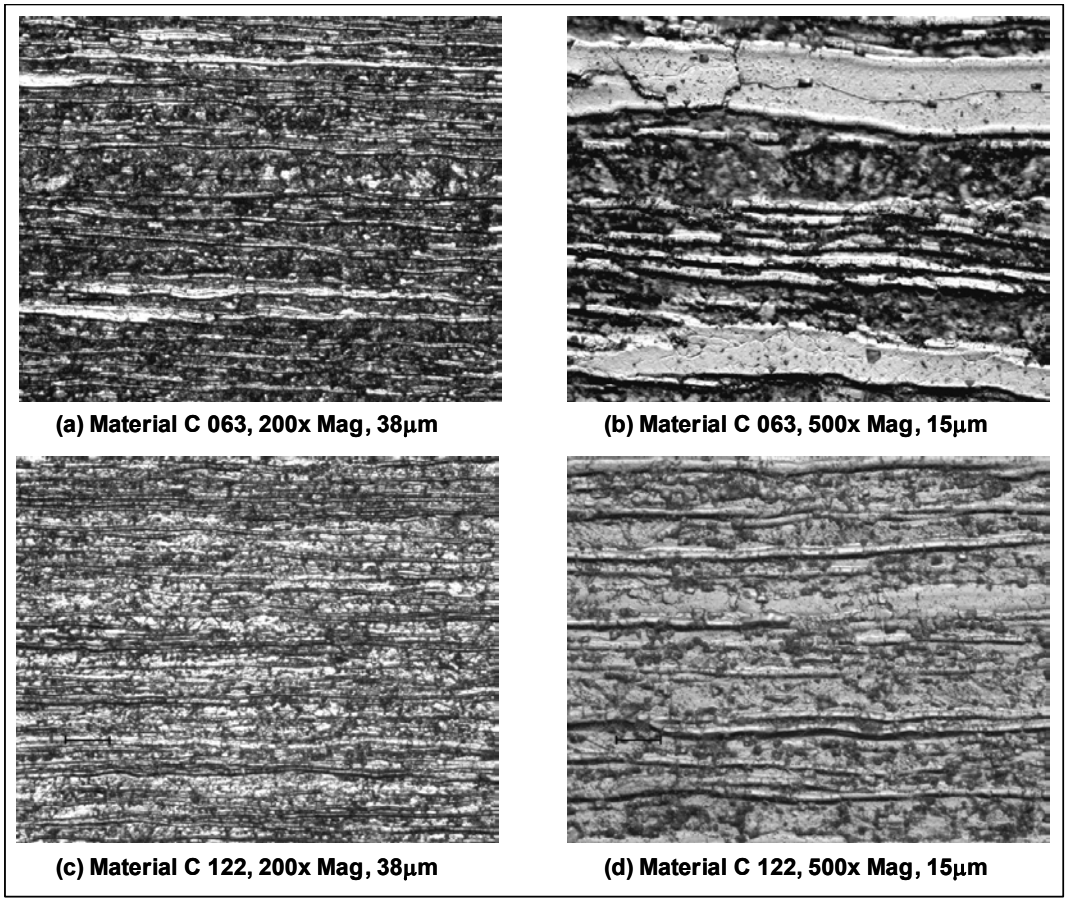

Figure 50 : Microstructures Of EPR Samples For Material C 063 And 122

As mentioned previously, the level of general corrosion on the samples from material C appears to be greater than on material A, probably due to the lower alloying content. Judging from the relatively higher Ir/Ia readings, the level of sensitisation is also likely to be higher. The micrographs shown in Figure 50 show very similar microstructures to the results obtained from the Strauss tests in that islands of δ ferrite remain relatively unattacked while the martensite matrix is extensively corroded. The extent of general and intragranular corrosion on the samples depicted in Figure 50 is very similar to the corrosion seen on samples from material A with similar Ir/Ia ratios.

Two examples of the EPR scans are shown in Figure 51 and Figure 52. Both of these curves show the typical martensite reactivation shoulder but also show a very clear grain boundary reactivation peak, despite the extensive general corrosion shown in the micrographs. Unfortunately such clear curves were not obtained for all the tests and the martensite reactivation shoulder was blurred by noise. Due to the inherently low corrosion resistance of the material, extensive gas generation on the surface of the samples occurred, which leads to excessive noise and current fluctuation.

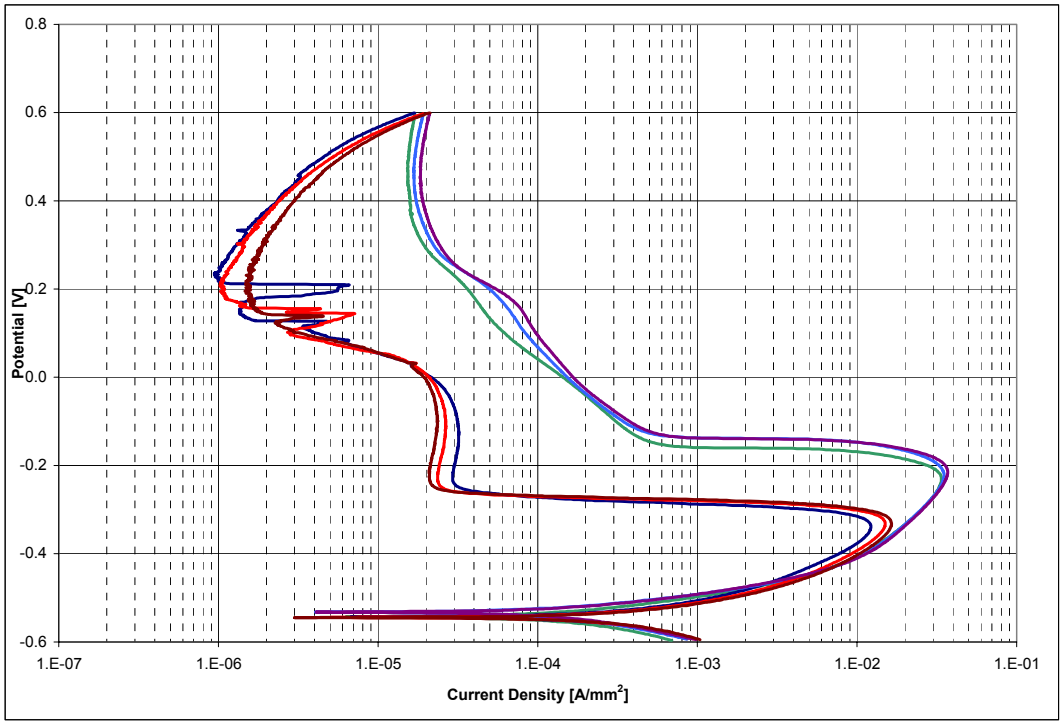

Figure 51 : EPR Scan Of Material C122

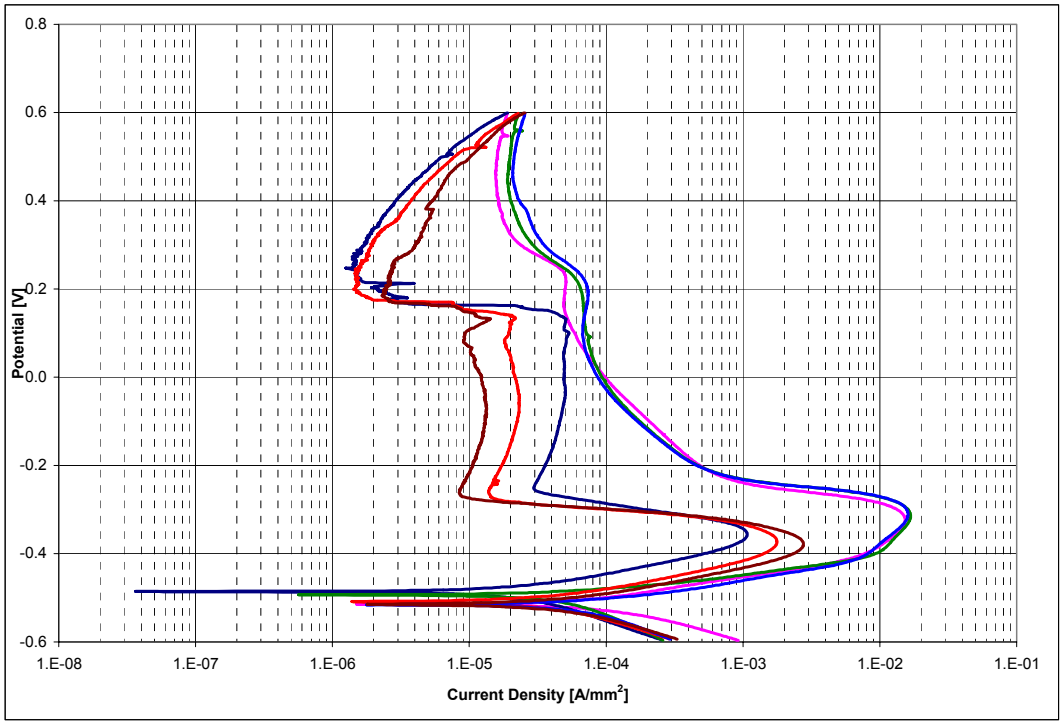

Figure 52 : EPR Scan For Material A 092

4.2.1.3 EPR Discussion

The EPR data from the welded samples does not result in any correlation between the degree of sensitisation and the heat input, predominantly because a sufficiently large array of samples wasn't available. Only two samples from each material was selected (as shown in Table 6) and the two samples used from material A had very similar welding conditions. The main criterion for selecting samples for EPR testing was that the weld integrity was acceptable and that didn't leave very many samples available to choose from. Welds with obvious defects like excessive overlap or large heat affected zones which obviously reached the surface had to be excluded. The intention of the EPR tests was to look for the presence of mode 4 sensitisation and samples where significant mode 2 sensitisation would have been present would defeat the purpose. However, with hindsight, the experimental procedure for this test could have been dramatically

simplified. The metallographical examinations (specifically the results from etching in oxalic acid) show that very little interaction occurs between the last pass (pass 8) and the two previous passes (6 or 7) at the edges of the V as in Figure 14, provided the passes have been positioned accurately. Therefore, similar sensitisation results should be achievable with a single weld bead which would enable rapid generation of a much larger sample set with much greater control on the welding parameters and corresponding consistency. However, once the results from the planned set of experiments had been completed, insufficient time was available to attempt the revised programme.

From the results shown in Table 6, the greatest anomaly is the fact that the base metal sample has a significantly larger current density ratio than the other samples from the same test piece. Since the base metal should not contain any sensitised regions, it would be expected that the Ir/Ia ratio be less than the results from any sample with sensitised grain boundaries and correspondingly higher dissolution rate. The result for sample A109/1 is possibly suspect since it should correlate well with the sample obtained from the Gleeble simulation results, since it is inherently the same material. However, as shown in Table 7, the results differ by a factor of roughly 20. Since the remaining samples are a lot closer to the results given in Table 7, it is likely that any error occurred on sample A109.

One very useful result which came out of the EPR work on the welded samples was the clear indication that mode 4 sensitisation was occurring on both materials, even though very little evidence of it could be detected by the Strauss tests or even the metallographic examination afterwards. However, as shown in Figure 41, evidence of

mode 4 sensitisation can be seen with minimal magnification and similar results were visible on samples from both materials. However, as indicated, the degree of attack was minimal and no evidence of intergranular attack penetrating into the material could be detected. The micrographs in Figure 42 and subsequent figures show that a fine line with grain boundary corrosion does exist and this is potentially a problem. In their review of testing methods, Clarke et al [49] maintained that residual stresses are a significant factor in determining whether IGC will occur in a marginally sensitised region. The test conditions as outlined for these experiments are obviously designed with the express purpose of inducing as much corrosion in the shortest possible time. In a practical application, proper post welding treatment involving pickling and passivation could result in faultless operation for the intended life of the structure. High bending stresses and excessively corrosive environments could however result in cracks initiating at the corroded grain boundaries and propagating along the edge of the HAZ. The risk of IGC along the subcritical HAZ would have to be weighed up against the additional cost and manufacturing issues associated with producing stabilised heavy gauge shear plate.

The fact that obvious mode 4 sensitisation could be detected on both materials is probably the most significant result to come out of the tests. The currently proposed theory [27] for mode 4 sensitisation states that low Ac_1 material should not suffer from mode 4 since no dissolution and subsequent reprecipitation of carbides (with the associated chromium depletion) should be occurring at temperatures below 770 – 780°C. Any carbon released by carbide dissolution above the Ac_1 would be absorbed by the austenite and remain in the martensite and therefore circumvent any grain boundary precipitation. On the other hand, at temperatures marginally above the Ac_1, the volume

of γ created would be small and restricted to the grain boundary regions of the existing martensite. On cooling, regions of untempered martensite would then be created on the grain boundaries and these regions might be preferentially corroded. The corrosion pattern in Figure 44(b) has the appearance of pitting surrounding the large δ ferrite grains rather than typical IGC. This could possibly be attributed to localised attack on grain boundary martensite. The presence of untempered martensite would be very difficult to detect since it would be created in a very limited region and in small quantities and would require SEM investigation to confirm.

Overall, the general level of consistency and repeatability over all the EPR results left a lot to be desired. Problems were experienced with gas bubbles forming in the SCE and excessive gas generation from the sample surface, which would have resulted in extensive fluctuations in the current reading. More scans at different scanning rates would probably have resulted in more reliable data.

In order to obtain an accurate evaluation of the EPR results and the degree of sensitisation, a much more rigorous testing routine would be required. The actual Ac_1 temperature of the materials will have a significant impact on the degree of sensitisation observed and as such samples would need to be heat treated at different temperatures and different cooling rates in order to observe which effects have the greatest impact on the presence of sensitisation. These tests would need to include temperatures as close to the Ac_1 as possible, both above and below the Ac_1 temperature. However, the number of samples required to obtain a respectable matrix of data to provide a full evaluation was beyond the scope of this project.

The EPR experiments provided some of the most interesting results for the whole project. Despite the variation seen in the scans, activation and reactivation potentials could be determined in all but a few instances, in which case the test was repeated. The tests on both the actual and simulated welds showed that low levels of sensitisation could be detected. Despite the scatter in the results shown in Figure 46, some correlation between the cooling rate and the degree of sensitisation can be seen and it is probable that better control of the reheat temperature and a larger sample set would provide much better correlation. Further investigation using the scanning reference electrode technique (SRET) as described by Vyas [50] would probably produce very interesting results, specifically on welded samples.

4.3 General Discussion

All the results from the various tests lead to the same conclusion that all forms of sensitisation cannot be avoided or eliminated in the alloys under investigation by suitable selection of the welding parameters. Mode 1 sensitisation will not occur in practice if the parent material has not been heated above the austenitising temperature before fabrication and the material is free from untempered martensite. As such, mode 1 is not relevant to this project.

Mode 3 has been shown [27, 38] to be attributable to very rapid cooling rates resulting from low heat input and weld cusps and significantly affects steels with high ferrite factor. As such, from the ferrite factor data given in Table 2, all the tested materials should be susceptible to mode 3 sensitisation under appropriate conditions. However, mode 3 sensitisation was not identified in any of the experimental work done for this

project. This was to be expected since the range in the heat input would not have resulted in the extremely rapid cooling rates required for mode 3 sensitisation to occur. Therefore the austenite potential of the material is adequate to ensure some austenite reversion will occur and prevent sensitisation from occurring on the δ ferrite grain boundaries. This does however not rule out the possibility that mode 3 sensitisation will occur at weld cusps or at arc strikes.

Mode 2 and mode 4 sensitisation were seen separately and in combination but will be addressed as separate issues. Mode 2 sensitisation was seen on all the welded samples where the HAZ from one bead overlapped the HAZ from a previous bead, as shown in several figures in the above report. The oxalic acid etch technique clearly showed where significant tempering of the HAZ martensite had occurred, and therefore gave a strong indication of where corrosion would be expected to occur. Even though the ASTM standards [42, 43] define an oxalic etching test, it is not considered suitable for low chromium steels and therefore did not conclusively indicate the presence of sensitisation on these materials. Furthermore, it is not suggested as an appropriate etching technique for 12%Cr steels with Kallings No 2 [41] and Picric acid [47] being the commonly recommended solutions. The oxalic acid etch with a very much shorter etching time was tried in an attempt to get a better picture of the grain boundary precipitation and the results were unexpected but highly informative. Mode 2 sensitisation was seen on all the areas which were indicated by the oxalic acid etch and the correlation between the etch pattern and the copper deposition during the Strauss test was extremely good. While some IGC was expected, the extent of the observed corrosion was surprising. As has been shown in several figures, overall corrosion of the martensite was the most commonly observed corrosion, rather than specific grain boundary attack. As is shown

in Figure 29, sensitisation is not occurring at the δ-ferrite grain boundaries but rather within the martensite grains. It is likely that chrome carbides are forming at the martensite lath boundaries at the appropriate temperature which results in a network of chromium depleted subgrain boundaries. The fact that a chromium depletion mechanism is responsible is confirmed by the fact that a healing heat treatment at 700°C restores the corrosion resistance and removes any sign of intergranular attack in the Strauss test.

Even though sensitisation could not be eliminated by reducing the heat input, it could be seen that reducing the size of the heat affected areas dramatically reduced the sensitised regions, as shown in Figure 24 . This indicates that any welding techniques like weaving, and high deposition consumables like flux cored wire, will result in inferior properties. However, the worst instances of sensitisation and corrosion could clearly be linked to poor welding, specifically bad bead positioning and excessive overlap on subsequent beads. As shown in Figure 36, positioning of the back pass is critical, so that the HAZ from the root pass is engulfed by the back pass. This should however not be a problem for a competent welder. Similarly, proper positioning of the cover passes will ensure that the sensitising isotherm intersects with the filler metal of the previous pass and not with the HAZ .

Evidence of mode 4 sensitisation was intermittently seen on the welded samples after the completion of the Strauss test. Copper deposition did not occur on areas where any observed corrosion could only be attributed to mode 4. This relates specifically to the two passes located at either end of the V-notch where the HAZ was not influenced by any subsequent welds. However, after light polishing some corrosive attack could be

seen at the extreme limit of the LTHAZ, as seen in Figure 37 and Figure 38. Mode 4 was generally not detected at these positions on material A but some indication of IGC could be seen after polishing on material C. However, as shown with the EPR experiments, mode 4 sensitisation has definitely occurred on material A, even at the lowest heat input levels. This is particularly relevant in that mode 4 was clearly seen in two steels of significantly different composition and with substantially differing Ac_1 temperatures. This would appear to indicate that some mechanism other than the dissolution of low melting carbides (specifically of vanadium) must be resulting in carbon being available for precipitation of chromium carbides on cooling. This mechanism has to be independent of material condition and heat treatment since mode 4 sensitisation appears after a single weld pass and apparently over a wide range of heat input. In theory, stabilised steels should be immune to this form of sensitisation since all carbon should be tied up with titanium or niobium. However, mode 4 sensitisation was only detected after the EPR tests and no similar study on stabilised grades has been found to positively confirm that these tests will not detect any sensitisation.

Overall, the electrochemical tests produced highly variable and somewhat inconclusive results. Even though the EPR technique is reported to provide quantitative results for the degree of sensitisation, which are supposed to be significantly more sensitive than the Strauss test or the other weight loss tests described in the ASTM standards, no definite correlation between the welding / simulation heat treatment cycles and the degree of sensitisation could be established. In practice, the EPR results showed some inconsistencies and a great deal of noise was seen on the plots, but some correlation between the current density ratio and the cooling rate could be seen. The inconsistencies

in the results are believed to be attributable to the variation seen during the Gleeble simulation rather than with the EPR test.

5 Conclusions

To summarise, unstabilised thick gauge 12%Cr steels are susceptible to mode 2 sensitisation but in the majority of cases this should not present a problem in service since the sensitised regions remain buried below the surface of the plate. Conditions which would exacerbate the problem need to be carefully controlled or avoided and these include high heat input, any techniques which result in very high metal deposition rates, inappropriate weld bead overlap and weaving or stop/start operation.

Mode 4 sensitisation was detected irrespective of heat input and material transformation temperature. However, low heat inputs and fast cooling rates will reduce the level of sensitisation. In addition, the level of mode 4 sensitisation is much lower than that observed for mode 2. As such, mode 4 is only likely to lead to service problems in severe corrosion environments in conjunction with high stress levels.

It all the immersion tests it could be seen that more copper deposited on the upper surface of the sample than on the same surface if the sample was positioned vertically. While the extent of copper deposition is not necessarily indicative of the extent of sensitisation, it does provide a measure of the amount of corrosion taking place. The actual mechanism by which corrosion is occurring is not particularly relevant but it does indicate that any form of fouling on the weld beads is likely to increase the chances of corrosion and therefore cleaning, pickling and passivation of the beads after welding is very important.

6 References

1. Bain, E.C., R.H. Arborn, and J.J.B. Rutherford, *The Nature and Prevention of Intergranular Corrosion in Austenitic Stainless Steels.* Transactions of American Society for Steel Treating, 1933. **21**: p. 481.
2. Nehrenberg, A.E. and P. Lillys, *High Temperature Transformations in Ferritic Stainless Steels containing 17 - 25% Chromium.* Transactions of the ASM, 1954. **46**: p. 1176 - 1203.
3. Irvine, K.J., D.J. Crowe, and F.B. Pickering, *The Physical Metallurgy of 12% Cr Steels.* Journal of the Iron & Steel Institute, 1960(8): p. 43-62.
4. Bond, A.P., *Mechanisms of Intergranular Corrosion in Ferritic Stainless Steels.* Transactions of the Metallurgical Society of AIME, 1969: p. 2127 - 2134.
5. Demo, J.J., *Mechanism of High Temperature Embrittlement and Loss of Corrosion Resistance in AISI Type 446 Stainless Steel.* Corrosion, 1971. **27**(12): p. 531-544.
6. Streicher, M., *The Role of Carbon, Nitrogen and Heat Treatment in the Dissolution of Iron-Chromium Alloys in Acids.* Corrosion, 1973. **29**(9): p. 337-360.
7. Demo, J.J., *Structure and Constitution of Wrought Ferritic Stainless Steels*, in *Handbook of Stainless Steels*, D. Peckner and I.M. Bernstein, Editors. 1977, McGraw-Hill Book Company. p. 5.1-5.40.
8. Campbell, R.G., *Ferritic Stainless Steel Welding Metallurgy.* Engineering Materials, 1992. **69/70**: p. 167-216.

9. Semchyshen, M., A.P. Bond, and H.J. Dundas, *Effects of Composition on Ductility and Toughness of Ferritic Stainless Steels*, in *The Metallurgical Evolution of Stainless Steels*, F.B. Pickering, Editor. 1972, ASM. p. 260-273.

10. Kaltenhauser, R.H., *Improving the Engineering Properties of Ferritic Stainless Steels.* Metals Engineering Quarterly, 1971. **11**(2): p. 41-47.

11. Folkhard, H., *Welding Metallurgy of Stainless Steels*. 1988, Vienna, Austria: Springer Verlag.

12. Gooch, T.G., *Corrosion Behaviour of Welded Stainless Steels.* Welding Journal, 1996. **75**(5): p. 135s - 154s.

13. Demo, J.J. and A.P. Bond, *Intergranular Corrosion and Embrittlement of Ferritic Stainless Steels.* Corrosion, 1975. **31**(1): p. 21-22.

14. Arai, H. and S. Takeda, *Theoretical Analysis of Grain Boundary Carbide Precipitation in Stainless Steels.* Tetsu to Hagane (Iron & Steel, Japan), 1986. **72**(7): p. 831-838.

15. Arai, H., S. Takeda, and Y. Arata, *Theoretical Analysis of Susceptibility of Ferritic Stainless Steel to Intergranular Corrosion caused by Welding.* Transactions of the JWRI, 1987. **16**(1): p. 131-137.

16. Nooning, R.G., *Effect of Stabilizing Elements on the Precipitation Behavior and Phase Stability of Type 409 Ferritic Stainless Steels*, in *School of Engineering*. 2002, University of Pittsburgh: Pittsburgh. p. 1-102.

17. Lee, Y.K., et al. *Effects of Annealing Temperature and Cooling Rate on the Grain Boundary Precipitation in Boron Added 304 Stainless Steels*. in *International Conference on Stainless Steels*. 1991. Chiba, Japan: ISIJ.

18. Barkleit, G., et al., *Analysis of intergranular corrosion attack on stainless steels by means of atomic force microscopy and optical microscopy Part 1: Influence of heat treatment.* Materials & Corrosion, 2000. **51**: p. 108-114.

19. Barkleit, G., et al., *Analysis of intergranular corrosion attack on stainless steels by means of atomic force microscopy and optical microscopy Part 2: Influence of impurity content.* Materials & Corrosion, 2000. **51**: p. 115-119.

20. Demo, J.J., *Weldable and Corrosion-Resistant Ferritic Stainless Steels.* Metallurgical Transactions A, 1974. **5**(11): p. 2253-2256.

21. Lula, R.A. and J.A. Davis, *Intergranular Corrosion in 12 Percent Chromium Ferritic Stainless Steels*, in *Intergranular Corrosion of Stainless Alloys, ASTM STP 656*, R.F. Steigerwald, Editor. 1978, ASTM. p. 233-247.

22. Gordon, W. and A. van Bennekom, *Review of Stabilisation of Ferritic Stainless Steels.* Materials Science & Technology, 1996: p. 126-131.

23. Ogwu, A.A. and T.J. Davies, *Improving the sensitization resistance of ferritic stainless steels.* Scripta Materialia, 1997. **37**(3): p. 259-263.

24. Fritz, J.D. and I.A. Franson, *Sensitization and stabilization of type 409 ferritic stainless steel.* Materials Performance, 1997. **36**(8): p. 57-61.

25. Dundas, H.J. and A.P. Bond, *Niobium and Titanium Requirements for Stabilization of Ferritic Stainless Steels*, in *Intergranular Corrosion of Stainless Steels, ASTM STP 656*, R.F. Steigerwald, Editor. 1978, American Society for Testing & Materials. p. 154-178.

26. Devine, T.M. and A.M. Ritter, *Sensitization of 12 Wt Pct Chromium, Titanium-Stabilized Ferritic Stainless Steel.* Metallurgical Transactions A, 1983. **14A**(8): p. 1721-1728.

27. Williams, J.G. and F.J. Barbaro. *Susceptibility and Prevention of HAZ Sensitisation and Intergranular Stress Corrosion Cracking in Various 12% Cr Steels*. in *AISTech 2005*. 2005. Charlotte, North Carolina, USA: AIST.

28. Gooch, T.G., P. Woollin, and A.G. Haynes, *Microstructural Development on Welding Low Carbon 13% Cr Martensitic Steels*. 1999, IIW Document, IX - H - 449 - 99. p. 1 - 15.

29. Wright, R.N., *Toughness of Ferritic Stainless Steels*, in *Toughness of Ferritic Stainless Steels, ASTM STP 706*, R.A. Lula, Editor. 1980, ASTM. p. 2-33.

30. Steigerwald, R.F., et al., *The Physical Metallurgy of Fe--Cr--Mo Ferritic Stainless Steels: A Review.* Metallurgist & Materials Technologist, 1978. **10**(4): p. 181-189.

31. Sedriks, A.J., *Effects of Alloy Composition and Microstructure on the Passivity of Stainless Steels.* Corrosion, 1986. **42**(7): p. 376-389.

32. Marshall, A.W. and J.C.M. Farrar, *Welding of Ferritic and Martensitic 11-14%Cr Steels*. 2000, IIW Document, IXH - 494 - 2000. p. 1-39.

33. Matthews, L.M., et al. *Sensitisation in Low-Carbon 12%Cr Containing Stainless Steels*. in *14th International Corrosion Congress*. 1999. Cape Town, South Africa: Corrosion Institute of Southern Africa.

34. Pistorius, P.G.H. and G.T. van Rooyen, *Composition and Properties of Ferritic Stainless Steels with Good Weldability.* Welding in the World, 1995. **36**(6): p. 65-72.

35. Knutsen, R.D., *Influence of Compositional Banding on Grain Anisotropy in 3CR12 Steel.* Materials Science & Technology, 1992. **8**(7): p. 621 - 627.

36. Matthews, L.M., et al. *A Review on the Welding and Weld Properties of 3CR12 Type Alloys*. in *IIW Asian Pacific Welding Congress, Proceedings*. 2000. Melbourne, Australia.

37. *Columbus Stainless - 3CR12 Technical Manual*. April 2001.

38. Greef, M.L. and M. Du Toit, *The Sensitisation of Two 11-12% Chromium Type EN 1.4003 Ferritic Stainless Steels During Continuous Cooling After Welding*. 2005, IIW Document, IX-2182-05. p. 1-11.

39. Miyakusu, K., H. Fujimoto, and T. Tanaka, *Ferrite and Martensite Dual Phase Stainless Steel NSS431DP-1*. 1989, Nisshin Technical Report. p. 115-121.

40. Gooch, T.G. and B.J. Ginn, *Heat Affected Zone Toughness of SMA Welded 12% Cr Martensitic-Ferritic Steels.* Welding Research Supplement, 1990(11): p. S431-S440.

41. Meyer, A.M. and M. Du Toit, *Interstitial Diffusion of Carbon and Nitrogen into Heat-Affected Zones of 11–12% Chromium Steel Welds.* Welding Research Supplement, 2001. **80**(12): p. S275 - S280.

42. ASTM A 262-98, *Standard Practices for Detecting Susceptibility to Intergranular Attack in Austenitic Stainless Steels*, in *Annual Book of ASTM Standards*, ASTM, Editor. 1998, ASTM: West Conshohocken, PA. p. 50-65.

43. ASTM A 763-93, *Standard Practices for Detecting Susceptibility to Intergranular Attack in Ferritic Stainless Steels*, in *Annual Book of ASTM Standards*, ASTM, Editor. 1993, ASTM: West Conshohocken, PA. p. 421-431.

44. Devine, T.M. and B.J. Drummond, *An Accelerated Intergranular Corrosion Test for Detecting Sensitization in Low Chromium Ferritic Stainless Steels.* Corrosion, 1982. **38**(6): p. 327-330.

45. Lee, J.B., *Modification of the ASTM Standard Ferric Sulfate--Sulfuric Acid Test and Copper--Copper Sulfate--Sulfuric Acid Test for Determining the Degree of Sensitization of Ferritic Stainless Steels.* Corrosion, 1983. **39**(12): p. 469-474.

46. Franson, I.A. and J.D. Fritz. *Stabilization requirements for T409 (UNS S40900) ferritic stainless steel*. in *Corrosion Prevention*. 1997. Detroit, Michigan; USA.

47. Pistorius, P.C. and M. Coetzee, *Sensitisation of Type 430 Ferritic Stainless Steel During Continuous Annealing.* Journal of the South African Institute of Mining and Metallurgy, 1996. **96**(3): p. 119-125.

48. Walker, W.L., *Variations in the Evaluation of ASTM A262, Practice E, Results (ASTM Subcommittee A01.14 Round Robin)*, in *Intergranular Corrosion of Stainless Alloys*, R.F. Steigerwald, Editor. 1978, American Society for Testing and Materials. p. 146 - 153.

49. Clarke, W.L., R.L. Cowan, and W.L. Walker, *Comparative Methods for Measuring Degree of Sensitisation in Stainless Steel*, in *Intergranular Corrosion of Stainless Alloys, ASTM STP 656*, R.F. Steigerwald, Editor. 1978, American Society for Testing and Materials. p. 99 - 132.

50. Vyas, B. and H.S. Issacs, *Detecting Susceptibility to Intergranular Corrosion of Stainless Steel Weld Heat-Affected Zones*, in *Intergranular Corrosion of Stainless Steels, ASTM STP 656*, R.F. Steigerwald, Editor. 1978, ASTM. p. 133-145.

51. Majidi, A.P. and M.A. Streicher, *The Double Loop Reactivation Method for Detecting Sensitization in AISI 304 Stainless Steels.* Corrosion, 1984. **40**(11): p. 584 - 593.

52. Frangini, S. and A. Mignone, *Modified Electrochemical Potentiokinetic Reactivation Method for detecting Sensitization in 12wt% Cr Ferritic Stainless Steels.* Corrosion, 1992. **48**(9): p. 715 - 726.

53. Alonso-Falleiros, N., M. Magri, and I.G.S. Falleiros, *Intergranular Corrosion in a Martensitic Stainless Steel Detected by Electrochemical Tests.* Corrosion, 1999. **55**(8): p. 769-778.

54. Smith, D.A.A. and J.N. Tarboton, *Personal Communication*. 2005, Columbus Stainless Pty Ltd.